

NITROUS OXIDE (N₂O) in MACQUARIE HARBOUR, TASMANIA

Maxey, Johnathan Daniel^{1,2}, Neil D. Hartstein², Hermann W. Bange³, Moritz Müller¹

¹Faculty of Engineering, Computing and Science, Swinburne University of Technology, Kuching 93350, Malaysia

²ADS Environmental Services, Kota Kinabalu, Sabah, 88400, Malaysia

³GEOMAR Helmholtz Centre for Ocean Research Kiel, Wischhofstr. 1-3, 24148 Kiel, Germany

Correspondence to: Johnathan Daniel Maxey, Neil D. Hartstein, Hermann W. Bange, and Moritz Müller

Abstract. Fjord-like estuaries are hotspots of biogeochemical cycling due to steep physicochemical gradients.

The spatiotemporal distribution of nitrous oxide (N₂O) within many of these systems is poorly described, especially in the southern hemisphere. The goal of this study is to describe the spatiotemporal distribution of N₂O within a southern hemisphere fjord-like estuary, describe the main environmental drivers of this distribution, the air/sea flux of N₂O, and the main drivers of N₂O production. [Sampling surveys](#)~~Cruises~~ were undertaken in Macquarie Harbour, Tasmania to capture N₂O concentrations and water column physicochemical profiles in winter (July 2022), spring (October 2022), summer (February 2023), and autumn (April 2023). N₂O samples were collected at one depth at system end members, and at 5 depths at 4 stations within the harbour.

Results indicate that N₂O is consistently supersaturated (reaching 170% saturation) below the system's freshwater lens where oxygen concentrations are often hypoxic, but infrequently anoxic. In the surface lens, levels of N₂O saturation vary with estimated river flow and with proximity to the system's main freshwater endmember. The linear relationship between [apparent oxygen utilization AOU](#) and ΔN₂O saturation indicates that nitrification is the process generating N₂O in the system. When river flow was high (July and October 2022), surface water N₂O was undersaturated (as low as 70%) throughout most of the harbour.

When river flow was low (February and April 2023) N₂O was observed to be supersaturated at most stations. Calculated air/sea fluxes of N₂O indicated that the system is generally a source of N₂O to the atmosphere under weak river flow conditions and a sink during strong river flow conditions. The diapycnal flux was a minor contributor to surface water N₂O concentrations, and subhalocline N₂O is intercepted by the riverine surface lens and transported out of the system to the ocean during strong river flow conditions. In a changing climate, Western Tasmania is expected to receive higher winter rainfall and lower summer rainfall which may augment the source and sink dynamics of this system by enhancing the summer / autumn efflux of N₂O to the atmosphere.

This study is the first to report observations of N₂O distribution, generation processes, and estimated diapycnal / surface N₂O fluxes from this system.

Formatted: Not Highlight

35 1. Introduction

Despite the fact that fjords and fjord-like estuaries represent only a small portion of the coastal area worldwide, they are responsible for sequestering 11% of the global organic carbon (C) burial along terrestrial margins (Smith *et al.*, 2015; Bianchi *et al.*, 2018, 2020). These systems are significant sources of greenhouse gasses (GHG) to the atmosphere (Wilson *et al.*, 2020; Rosentreter *et al.*, 2023; Bange *et al.*, 2024). Many are heavily stratified with strong water column physicochemical gradients (Acuña-González *et al.*, 2006; Inall and Gillibrand, 2010; Hartstein *et al.*, 2019; Salamena *et al.*, 2021, 2022; Maxey *et al.*, 2022). These gradients can be influenced by mesoscale climate drivers like North Atlantic Oscillation (NAO) and Southern Annular Mode (SAM) (see Austin and Inall 2002; Gillibrand *et al.*, 2005; Maxey *et al.*, 2022) and local scale drivers like fresh water input and marine intrusions (Inall and Gillibrand 2010; Hartstein *et al.*, 2019; Maxey *et al.*, 2020; Salamena *et al.*, 2022).

Nitrous oxide (N₂O) is a potent GHG whose increased presence in the atmosphere is primarily driven by emissions from agricultural soils with an increased presence in poorly oxygenated marine systems (Laffoley and Baxter 2019; Ji *et al.*, 2020; Wilson *et al.*, 2020; Wan *et al.*, 2022; Orif *et al.*, 2023). With a global warming potential nearly 300 times that of CO₂ (Myhre *et al.*, 2013; Etminan *et al.*, 2016; Eyring *et al.*, 2021; Forster *et al.*, 2021) N₂O is a key focus of climate studies especially regarding ozone layer depletion. N₂O is a precursor to NO, and a major ozone depleting substance in the atmosphere (Nevison and Holland, 1997; Ravishankara *et al.*, 2009; Portmann *et al.*, 2012). N₂O production occurs through the microbially mediated processes of ammonia oxidation, nitrite (NO₂⁻) reduction, and nitrate (NO₃⁻) reduction (Kuypers *et al.*, 2018). N₂O production in marine systems is governed by environmental conditions such as dissolved oxygen (DO) availability, ammonium (NH₄⁺) availability, light availability, temperature (e.g. Raes *et al.*, 2016), pH (e.g. Breider *et al.*, 2019), and microbial community composition (e.g. Wu *et al.*, 2020).

60 2. Methods

2.1 Study Area

Macquarie Harbour is a southern hemisphere fjord-like estuary located on Tasmania, Australia's west coast (Figure 1). The harbour is oriented NW by SE, and is approximately 33 km long, 9 km wide, with a surface area of 276 km². The mouth of the harbour is constricted by a shallow (4-8m), long (14km) sill known as "Hells Gates". Hells Gates muffles tidal forcing resulting in harbour water levels primarily determined by river flow and wind set up (Hartstein *et al.*, 2019). The morphology of this system results in sharp gradients of DO, salinity, and temperature which are seasonally dependant (Creswell *et al.*, 1989; Hartstein *et al.*, 2019; Maxey *et al.*, 2022). In surface waters dissolved oxygen (DO) concentrations are nearly always in equilibrium with the air but decrease sharply through the halocline (~8m to 15m). There is almost no DO produced below the halocline (8m to 12m deep) due to high chromophoric dissolved organic matter (CDOM) levels limiting primary production at the surface (Maxey *et al.*, 2017, 2020). Subhalocline layers (~15m to a few meters from the bottom) are observed to have DO concentrations below 62.5 μM more than 50% of the time (see Maxey *et*

Formatted: Indent: First line: 0.63 cm

Formatted: Font: Bold

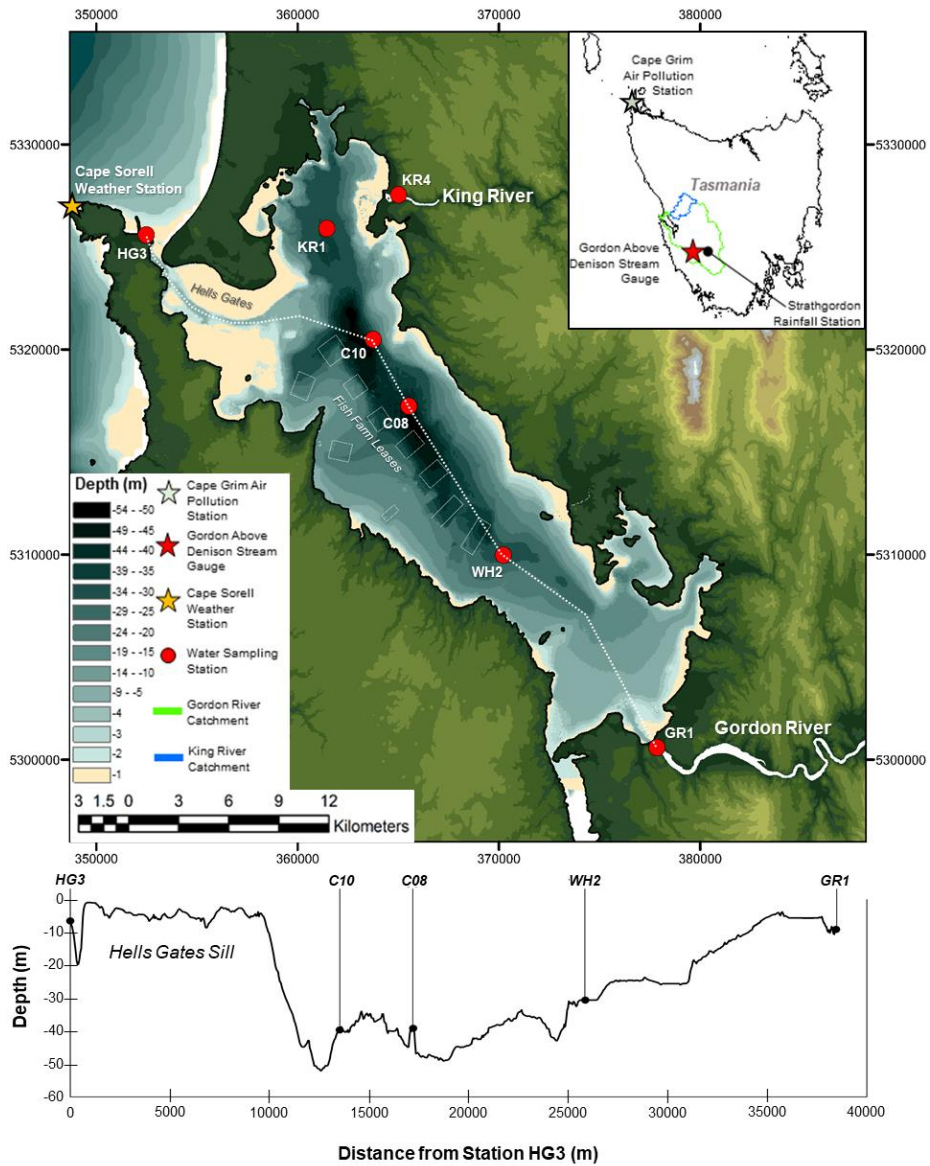
Formatted: Not Highlight

75 *al., 2022*). Near the seabed, episodic marine intrusions (deep water renewal) refresh the supply of DO near the mouth of the system but refresh the upper reaches of the harbour less frequently (see Andrewartha and Wild-Allen 2017; Hartstein et al., 2019; Maxey et al., 2022). This process is driven by low atmospheric pressure, sustained NW winds, and low catchment rainfall which itself is influenced by Southern Annular Mode (SAM) (Hartstein et al., 2019; Maxey et al., 2022). In the harbour's upper reaches DO concentrations fall below 31 μM nearly a third of the time (Maxey et al., 2022). Hydrodynamic and oxygen tracer numerical model simulations of the harbour by Andrewartha and Wild-Allen (2017) estimate that 50% of the harbour's basin waters are replaced every 65 days during low river flow conditions and approximately 110 days during normal flow conditions. In the upper reaches of the harbour marine intrusions are much less common (see Hartstein et al., 2019; Maxey et al., 2022). In these areas the DO concentration falls below 31 μM nearly a third of the time (Maxey et al., 2022).

80

Formatted: Not Highlight

Formatted: Not Highlight



85 **Figure 1: Macquarie Harbour, Tasmania. Water sampling stations shown with red circles; Cape Grim Air Pollution**
monitoring station shown as a green star (see inset map). Cape Sorell Weather Station shown as an orange star.
Gordon Above Denison stream gauge shown as a red star (see inset map). Aquaculture lease boundaries are shown as
hollow rectangles. Lease locations are sourced from Land Information Systems Tasmania (LISTmap -
<https://maps.thelist.tas.gov.au/>). Station names reflect general harbour locations where KR1 indicates King River 1;
 90 C10 and C08 indicate Central Harbour 10 and 08 respectively; WH2 indicates World Heritage Area 2; and GR1
 indicates Gordon River station 1. Coordinates are displayed in GDA_1994_MGA_Zone_55. Bathymetry through the
 system shown as a dashed line, note that this track excludes stations KR4 and KR1.

2.2 Experimental Design

Nitrous oxide distribution was assessed by collecting water samples across 7 stations, including the harbour's endmembers (mouths of the Gordon and King Rivers as well as the harbour mouth at Hells Gates Inlet; see Figure 1 and Table 1) and stations along the longitudinal axis of the harbour where the deepest basins are located (named KR1, C10, C08, and WH2). Samples collected at endmember stations were collected from a single depth as these stations are shallow. Samples in the harbour body were collected at 5 depths from the surface (2m) to approx. 1m from the seabed. Collection campaigns were conducted in July 2022, October 2022, February 2023, and April 2023. At each station and depth, three replicate vials (n = 3) were collected for the determination of N₂O concentration.

2.3 Field Sampling

At each station, water quality sonde profiles were collected from the surface to the seabed at 1 meter intervals using a YSI EXO-1 equipped with optical DO (accuracy from 0 to 625 µM ± 3 µM or 1% of reading whichever is greater; precision is 0.03 µM), salinity (accuracy ± 0.1 or 1% of reading whichever is greater; precision is 0.01), temperature (accuracy is ± 0.15 °C; precision is 0.01 °C), and depth sensors. Sonde calibration was checked and corrected (when needed) each sampling period.

Table 1: Sampling stations showing coordinates, parameters, and sampling depth (in meters).

Station	Station Depth (m) (MSL)	Dissolved Oxygen Salinity Temperature	N ₂ O	TAN (NH ₃ + NH ₄ ⁺)	NO ₃ ⁻
HG3 352484, 5325594	8	Every Meter	5m	5m	5m
KR4 365018, 5327550	3	1m	1m	1m	1m
KR1 361316, 5325972	36	Every Meter	2, 12, 20, 30, 35m	2, 12, 20, 30, 35m	2, 12, 20, 30, 35m
C10 363708, 5320464	44	Every Meter	2, 12, 20, 30, 42m	2, 12, 20, 30, 42m	2, 12, 20, 30, 42m
C08 365489, 5317238	47	Every Meter	2, 15, 25, 35, 45m	2, 15, 25, 35, 45m	2, 15, 25, 35, 45m
WH2 370218, 5309894	32	Every Meter	2, 12, 20, 25, 30m	2, 12, 20, 25, 30m	2, 12, 20, 25, 30m
GR1 377784, 5300603	12	Every Meter	10m	10m	10m

2.4 Analysis of Rainfall and River Loading Estimation

River loading and Rainfall and river discharge were analysed using methods presented in Maxey *et al.* (2022) where rainfall and stream gauge data were collected from the Gordon River catchment, Strathgordon

rainfall gauge station and the Gordon Above Denison (GAD) stream gauge (Figure 1). The rainfall and flow metrics computed include the average daily rainfall over a 20-day period prior to sampling; total accumulated rainfall 20, 10, 5, and 3 days prior to sampling; estimated Gordon River flow into the estuary; and measured flow at the GAD stream gauge.

2.5 Analysis of Water Column N₂O Concentrations, Air/Sea Flux, and Diapycnal Flux

2.5.1 Determination of N₂O Concentrations

Water samples were analysed for N₂O using the static-headspace equilibration method followed by gas chromatographic separation (HP Agilent 5890) and detection with an electron capture detector (ECD) as described in Bange *et al.*, (2019), Bastian (2017), and Kallert (2017). The concentration of N₂O in the samples was calculated with the following equation (Equation 1; see Bange *et al.*, 2006):

$$C_{\text{obs}} = \frac{x' PV_{\text{hs}}}{RTPV_{\text{wp}}} + X'\beta P$$

C_{obs} is the concentration (nmol L⁻¹) of N₂O in the water sample; x' is the measured dry mole fraction of N₂O in the sample vial's headspace; P is the ambient pressure set to 1 atm; V_{hs} and V_{wp} are the volumes of the headspace in the vial and water in the vial; R is the gas constant; T is the temperature during equilibrium; and β is the solubility of N₂O (Weiss and Price, 1980). The mean relative error of the concentration values obtained was 2.4% (± 0.16).

2.5.2 Estimation of N₂O Air/Sea Fluxes and N₂O Saturations

N₂O air/sea fluxes (F in $\mu\text{mol m}^{-2} \text{d}^{-1}$) were estimated using equations from Zhang *et al.*, (2010) and Bange *et al.*, (2019) (Equation 2) Where:

Equation 2

$$F = K * (C_{\text{obs}} - C_{\text{eq}})$$

C_{obs} is the measured concentration (nmol L⁻¹) of N₂O in the water sample; C_{eq} is the air-equilibrated seawater N₂O concentration, calculated for in situ temperature and salinity using the solubility data of Weiss and Price (1980). K is the gas transfer velocity, which in the absence of direct measurements can be expressed as a function of the wind speed and the Schmidt Number (Sc). For this study we sourced daily average wind speed from the Cape Sorrel Weather Station at the northern end of Macquarie Harbour (<http://www.bom.gov.au/climate/data/index.shtml> station ID 097000; see Figure 1 for station location). K was estimated using relationships in Nightingale (2000), Raymond and Cole (2001), and Wanninkhof (2014). Fluxes at Macquarie Harbour's endmember stations used K values that account for additional forcings like bottom shear (see Raymond and Cole 2001; Zappa *et al.*, 2003; Abril and Borges

Formatted: Indent: First line: 1.27 cm

Formatted: Font: Bold

Formatted: Font: Not Italic

Formatted: Font: Not Italic

Formatted: Font: Not Italic

Formatted: Font: Not Italic

Formatted: Font: Not Italic

Formatted: Font: Not Italic

Formatted: Indent: First line: 1.27 cm

Formatted: Font: Not Italic

Formatted: Font: Bold

Formatted: Font: Not Italic

Formatted: Font: Not Italic

Formatted: Font: Not Italic

Formatted: Font: Bold

Formatted: Font: Not Italic

Formatted: Font: Bold

Formatted: Font: Bold

Formatted: Font: Not Italic

2004, Beaulieu *et al.*, 2012; Rosentreter *et al.*, 2021). Deeper stations in the harbour's main body (*i.e.* KR1, C10, C08, WH2) have surface layers which are separated from the seabed by more than 10 meters. A wind-based K_{600} estimator was used to estimate air-sea flux in those locations (see Nightingale 2000; Raymond and Cole 2001; Wanninkhof 2014). Atmospheric N_2O for this estimation was sourced from monthly mean baseline greenhouse gas mole fractions measured at the Kennaook / Cape Grim Baseline Air Pollution Station, located in north west Tasmania. This station measures atmospheric N_2O using a gas chromatograph (GC) equipped with an ECD (<https://www.csiro.au/en/research/natural-environment/atmosphere/latest-greenhouse-gas-data>). N_2O saturation (in %) were computed as N_2O saturation = $100 * (C_{obs} / C_{eq})^+$.

Formatted: Font: Bold

2.5.3 Estimation of Diapycnal N_2O Flux

N_2O diapycnal fluxes (F_{dia} ; Equation 3) from basin waters (sample depths of 20m or 25m) to the harbour's surface lens (sample depths of 2m) were estimated as:

Equation 3

$$F_{dia} = K_{\rho} \frac{d[N_2O]}{dz}$$

Where z is depth. Diapycnal diffusivity (K_{ρ} ; Equation 4) was computed with the local buoyancy frequency (N^2), Γ set to 0.2 (Osborn 1980), and ϵ the dissipation rate of turbulent kinetic energy assumed to be on the upper end of values for the mixing zone of stratified systems 1×10^{-5} (Arneborg *et al.*, 2004; Mickett *et al.*, 2004; Fer *et al.*, 2006).

Equation 4

$$K_{\rho} = \Gamma \frac{\epsilon}{N^2}$$

Formatted: Font: Not Italic

Formatted: Font: Not Italic

Formatted: Font: Bold

Formatted: Font: Not Italic

Formatted: Font: Not Italic

Formatted: Font: Bold

2.6 Data Analysis

The relationships between N_2O saturation and water quality parameters such as DO concentration, salinity, temperature, nitrate, and ammonium concentrations determined using Pearson correlation. Differences in mean N_2O saturation between season, depth and each sampling station were tested using a 2-way ANOVA. Differences between rainfall / river flow metrics between seasons were tested using 1-way ANOVA and where significant differences between seasons were detected pair-wise testing using Bonferroni's correction was undertaken. The relationship between rainfall / river flow metrics, from the Gordon River, and surface water N_2O saturation / N_2O air/sea flux, at each station, was analysed using Pearson correlation. Standard deviation (std. dev.) of the mean air/sea flux and diapycnal flux was computed from error propagated from replicate observations of N_2O wind speed, N_2O concentration, and density (where appropriate) using methods from Ku (1966). Contour plots were made with Plotly Chart Studio: Plotly Technologies Inc. Title: Collaborative data science Publisher: Plotly Technologies Inc. Place of publication: Montréal, QC Date of publication: 2015 URL: <https://plot.ly> were analysed using Pearson correlation. The effects of season and depth on N_2O saturation at each sampling station was tested using a 2-way ANOVA. The relationship between rainfall / river flow metrics from the Gordon River and surface water N_2O saturation / N_2O air/sea flux at each station was analysed using Pearson correlation.

Formatted: Indent: First line: 0.63 cm

Formatted: Not Highlight

Formatted: Not Highlight

Formatted: Not Highlight

Formatted: Not Highlight

Formatted: Not Highlight

3. Results

3.1 Rainfall and River Loading

Twenty-day rainfall accumulation ranged from a low of 117 mm in July 2022 to a high of 139 mm in April 2023 with no detectable seasonal differences (see [Figure 2](#) [Figure 2A](#)). Average (\pm se) daily rainfall was similar across all months and ranged from 5.12 (\pm 2.57) mm in July 2022 to 5.79 (\pm 3.03) mm in October 2022 (see [Figure 2](#) [Figure 2B](#)) with no seasonal differences detected ($p = 0.4326$). As observed with accumulation metrics no seasonal differences were detected.

3.2 Water Column Physicochemical Profiles

DO profiles at the stations located within the main body of the harbour show a well oxygenated surface layer that rapidly attenuates with depth ([Figure 3](#) [Figure 3A](#)) through the halocline ([Figure 3](#) [Figure 3B](#)). There is a prominent riverine surface lens in the main harbour extending to depths of up to 8m depending on sampling period and location within the estuary. Salinity in the surface waters was lower in July and October 2022 (6 to 13) than February and April 2023 (greater than 20). Below the halocline salinity ranged from approx. 28 to 32.

The DO gradient between the surface and subhalocline waters was steeper in October relative to July 2022 with October 2022 DO concentrations approaching single digits (3.1 μ M) at station WH2, nearest the Gordon River mouth (see [Figure 1](#) [Figure 1](#)). In general, the subhalocline concentrations of DO were lower with proximity to the Gordon River mouth. The temperature of the freshwater surface layer ranged from about 9 °C to 19 °C, but showed little variation below the halocline where temperature ranged between 13 °C to 16 °C ([Figure 3](#) [Figure 3C](#)).

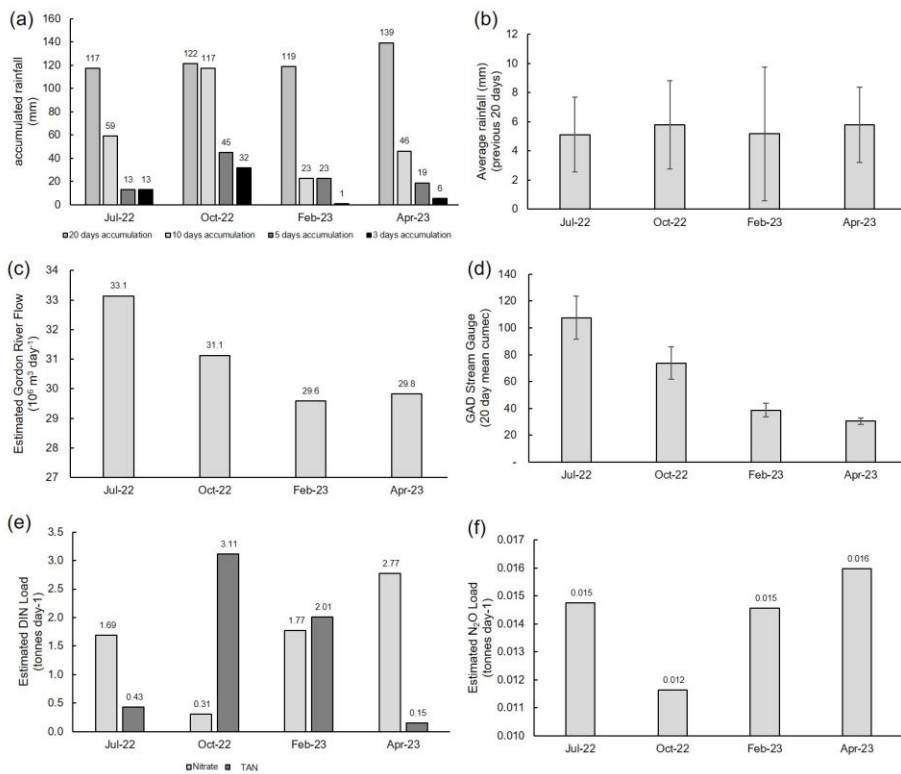
Nitrate concentrations in the surface water lens tended to be lower than those observed at subhalocline depths ([Figure a](#)). The greatest NO_3^- concentrations were observed 2m above the seabed at station WH2 in July and October 2022 as well as mid basin depths at stations C10 and C08 during those same periods with concentrations reaching 1.77 μ mol. TAN concentrations were often observed below detection limits (0.3 μ mol), but were greatest in the surface lens or within the halocline itself when detectable ([Figure b](#)). TAN concentrations at WH2 tended to be found at higher levels through the water column relative to other stations (down to about 20m) reaching 1.53 μ mol at 15m in October.

Formatted: Indent: First line: 0.63 cm

Formatted: Font: Bold

Formatted: Font: Bold

Formatted: Indent: First line: 0.63 cm



220 **Figure 2: Rainfall and estimated Gordon River loading estimates for each sampling event. A) accumulated rainfall**
 225 **(mm) 10, 5, and 3 days prior to each sampling event; B) average (mean) daily rainfall over a 20 day period prior to**
each sampling event; C) estimated Gordon River Flow into the harbour in millions of $\text{m}^3 \text{ day}^{-1}$; D) daily mean flow
($\text{m}^3 \text{ sec}^{-1}$) over previous 20 days prior to sampling (\pm standard error) at the Gordon Above Denison Stream Gauge; E)
estimated nitrate and ammonium loads entering the harbour from the Gordon River; F) estimated N_2O load (tonnes
 day^{-1}) entering the harbour from the Gordon River.

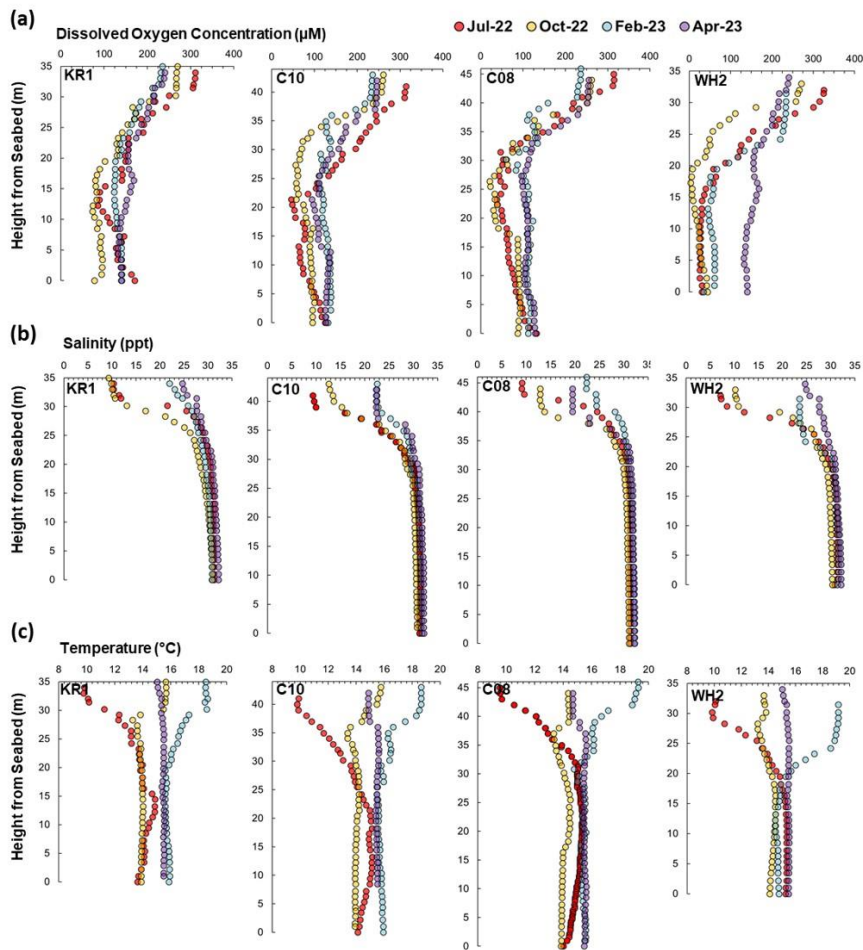


Figure 3: Dissolved oxygen (μM) (Row A), salinity (Row B), and temperature ($^{\circ}\text{C}$) (Row C) profiles (referencing height from seabed) collected at stations KR1, C10, C08, and WH2 in July 2022 (red dots), October 2022 (yellow dots), February 2023 (blue dots), and April 2023 (purple dots). Measurements were made every 1 meter.

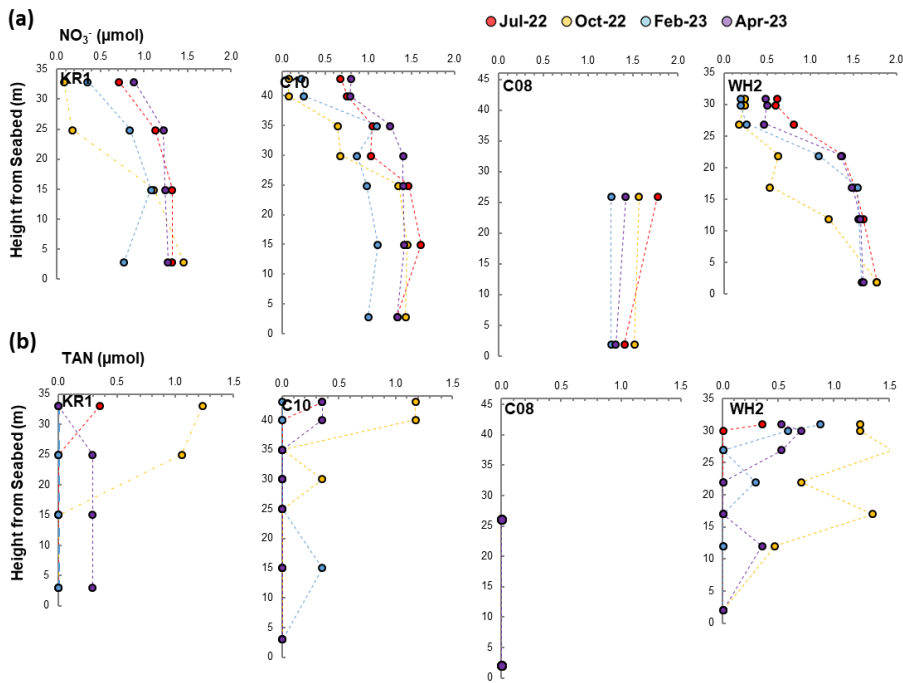


Figure 4: Nitrate NO_3^- (row a) and TAN (row b) concentrations with depth (referencing height from seabed) collected at stations KR1, C10, C08, and WH2 in July 2022 (red dots), October 2022 (yellow dots), February 2023 (blue dots), and April 2023 (purple dots). Data presented as having a concentration of 0.0 are below the detection limits of the analyte.

Formatted: Caption

Formatted: Superscript

3.3 N_2O Distribution

At each harbour station, depth and season (and their interaction) significantly impacted N_2O saturation (two-way ANOVA, $\alpha = 0.05$, degree of freedom ($d.f.$) = 59). At 2 m, N_2O saturation was observed to be below 100% at all stations in July 2022 (Figure 5 and Figure 6) and at stations KR1, C10, and C08 in October 2022. In February and April 2023 N_2O saturation in the harbour was above 100% through the water column except in KR1 surface waters. The maximum N_2O concentrations were observed in the subhalocline. Among the subhalocline observations the maximum N_2O concentrations (reaching over 170%) were observed at the base of the Hells Gates sill at station C10 in October 2022.

All endmember N_2O concentrations were undersaturated in July 2022. In October, stations KR1 and HG3 were observed to be approx. 100% saturated but N_2O at station GR1 was undersaturated. In February and April 2023 N_2O concentrations were supersaturated at all endmember stations. There were statistically significant linear correlations between N_2O saturation and salinity ($r = 0.494$; $p = 5.5 \times 10^{-7}$, $n = 92$), temperature ($r = 0.391$; $p = 1.2 \times 10^{-4}$, $d.f. = 90$), DO concentration ($r = -0.563$; $p = 5.2 \times 10^{-9}$, $d.f. = 90$), and nitrate concentration ($r = 0.559$; $p = 6.9 \times 10^{-9}$, $d.f. = 90$) in the harbour stations (Figure 7). The correlation between N_2O saturation and the TAN concentration however was not statistically significant ($r = 0.174$; $p = 0.31$, $d.f. = 34$).

Formatted: Indent: First line: 0 cm

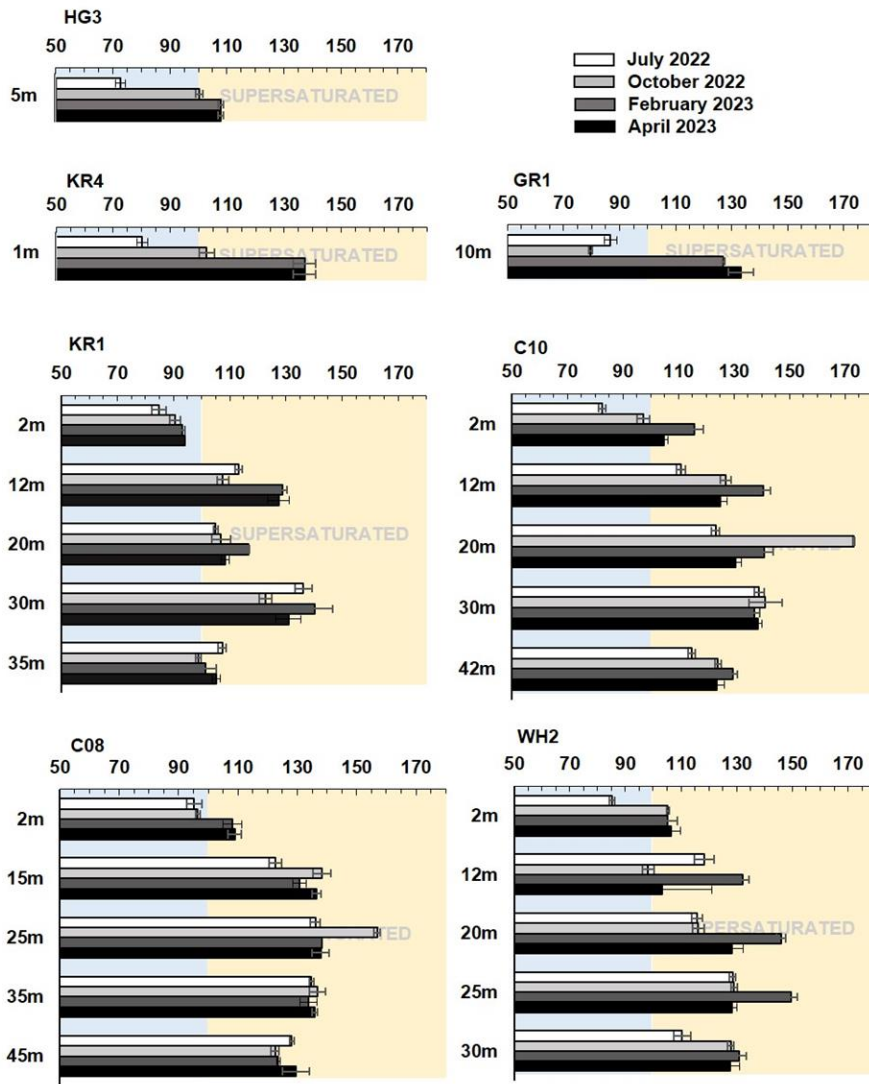
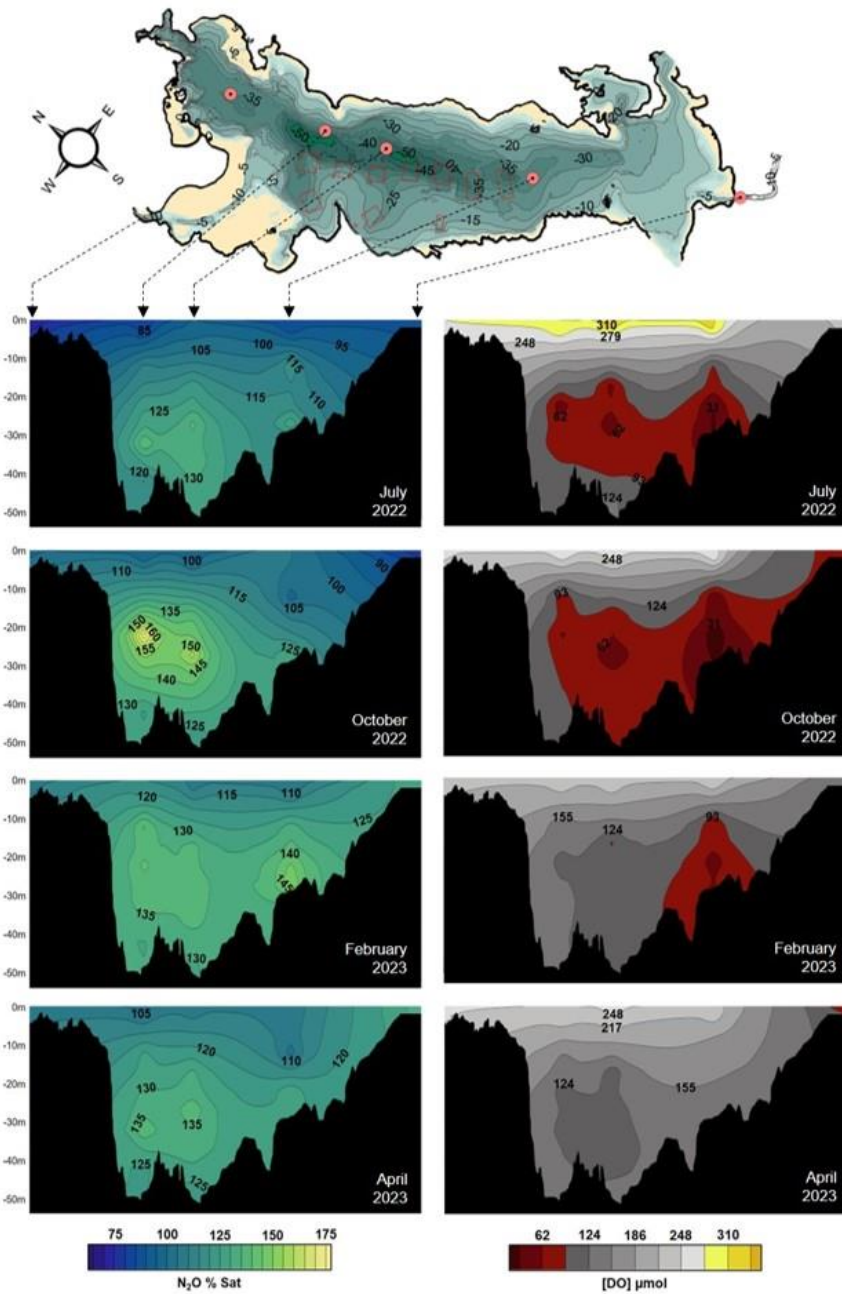
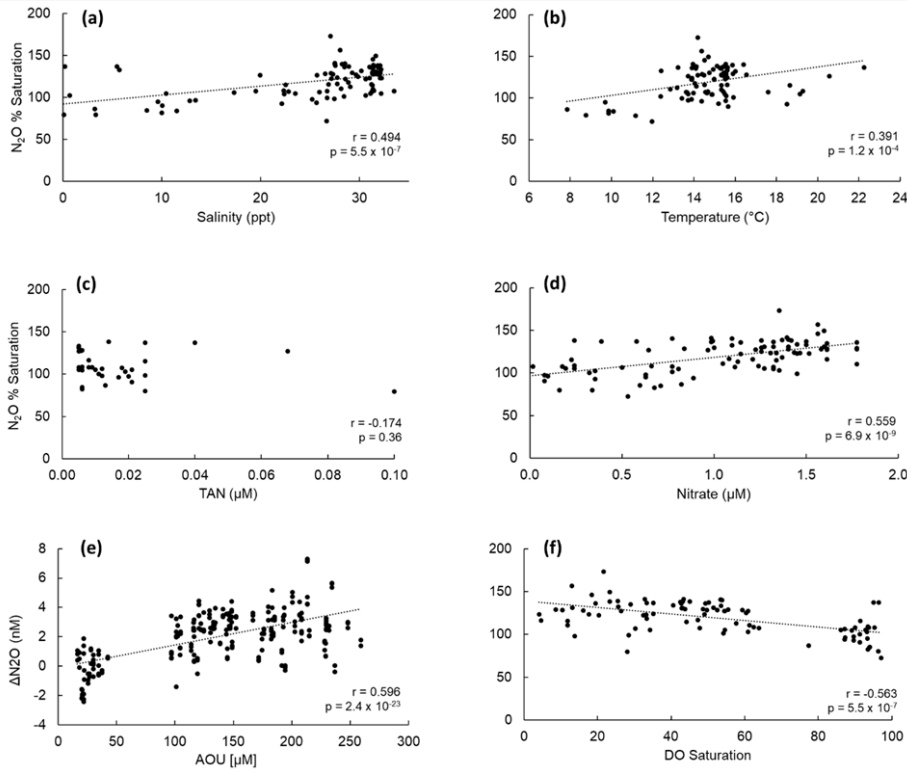


Figure 5: Mean (\pm standard error) N_2O % saturation observed at each sampling station, with depth, and across seasons. Note that a red dashed line indicating 100% at the time of sampling has been placed on each panel for reference.



255

Figure 6: Contour plots of mean N₂O % saturation (left column) and mean DO concentration in units of μmol (right column) observed at stations HG3, C10, C08, WH2, and GR1 from July 2022 to April 2023. Red shaded areas on the DO plots indicate low oxygen concentrations (< 93 μmol). Relative positions of the stations are shown on the top left panel. Y-axis displays depth in metres relative to mean sea level.



Formatted: Normal

Figure 75: Correlation between N₂O % saturation observed across the harbour and a) Salinity, b) Temperature, c) Total Ammoniacal Nitrogen (TAN) concentration, d) Nitrate concentration. The correlation between AOU [µM] and ΔN₂O [nM] is shown in panel e). The relationship between N₂O % saturation and DO % saturation is shown in panel f). Pearson correlation coefficients (r) and their associated p value are shown in each panel.

Formatted: Not Highlight

3.4 N₂O Air/Sea and Diapycnal Fluxes

Atmospheric N₂O mole fractions measured at Kinnaook / Cape Grim Air Pollution Station (see **Figure 1**) were observed to increase from 334.7 ppb in July 2022 to 335.9 ppb in February 2023. The April 2023 atmospheric N₂O mole fraction was slightly lower than that observed in February 2023 at 335.6 ppb. Average (± std. dev.) wind speeds were observed to be 6.6 (± 3.7) m sec⁻¹ in July, 5.6 (± 2.5) m sec⁻¹ in October, 6.3 (± 3.4) m sec⁻¹ in February, and 6.4 (± 4.0) m sec⁻¹ in April.

Formatted: Font: Bold

Station	K ₆₀₀	Jul 2022	Oct 2022	Feb 2023	Apr 2023	Gordon Flow	GAD Flow	GAD Flow	Rainfall
		µmol N ₂ O m ⁻² dav ⁻¹	µmol N ₂ O m ⁻² dav ⁻¹	µmol N ₂ O m ⁻² dav ⁻¹	µmol N ₂ O m ⁻² dav ⁻¹	vs Surface Flux	vs Surface Flux	vs % N ₂ O Sat.	vs Surface Flux

Formatted: Superscript

Formatted: Superscript

Formatted: Superscript

Formatted: Superscript

KR1	RC _{High} :	-11.07 ± 5.17	-04.01 ± 1.77	-03.30 ± 1.54	-03.17 ± 1.66	r = -0.8316 p = 7.5 x 10 ⁻⁴	r = -0.8624 p = 3.1 x 10 ⁻³	r = -0.8726 p = 2.1 x 10 ⁻⁴	r = 0.5577 p = 0.060
	RC _{Mid} :	-08.45 ± 4.42	-03.19 ± 1.59	-02.55 ± 1.34	-02.44 ± 1.41				
	RC _{Low} :	-04.69 ± 3.17	-01.93 ± 1.27	-01.46 ± 0.99	-01.38 ± 0.99				
	N ₂₀₀₀ :	-0.85 ± 0.31	-0.30 ± 0.08	-0.25 ± 0.09	-0.24 ± 0.11				
	W ₂₀₁₄ :	-0.78 ± 0.25	-0.27 ± 0.05	-0.23 ± 0.07	-0.22 ± 0.09				
C10	RC _{High} :	-12.88 ± 6.00	-01.21 ± 0.53	07.31 ± 3.43	02.60 ± 1.36	r = -0.8298 p = 8.4 x 10 ⁻⁴	r = -0.9091 p = 4.2 x 10 ⁻³	r = -0.8795 p = 1.6 x 10 ⁻⁴	r = 0.2751 p = 0.387
	RC _{Mid} :	-09.83 ± 5.14	-00.96 ± 0.48	05.65 ± 2.98	02.00 ± 1.16				
	RC _{Low} :	-05.46 ± 3.68	-00.58 ± 0.38	03.22 ± 2.19	01.13 ± 0.81				
	N ₂₀₀₀ :	-0.99 ± 0.36	-0.09 ± 0.02	0.67 ± 0.23	0.20 ± 0.09				
	W ₂₀₁₄ :	-0.91 ± 0.29	-0.08 ± 0.02	0.61 ± 0.18	0.18 ± 0.07				
C08	RC _{High} :	-03.50 ± 1.63	-01.69 ± 0.74	04.08 ± 1.91	04.57 ± 2.40	r = -0.8547 p = 3.97 x 10 ⁻⁴	r = -0.8804 p = 1.6 x 10 ⁻⁴	r = -0.8447 p = 5.4 x 10 ⁻⁴	r = 0.1846 p = 0.566
	RC _{Mid} :	-02.67 ± 1.40	-01.34 ± 0.67	03.15 ± 1.66	03.52 ± 2.03				
	RC _{Low} :	-01.49 ± 1.00	-0.81 ± 0.53	01.80 ± 1.22	01.98 ± 1.43				
	N ₂₀₀₀ :	-0.27 ± 0.10	-0.12 ± 0.03	0.31 ± 0.11	0.35 ± 0.15				
	W ₂₀₁₄ :	-0.25 ± 0.08	-0.11 ± 0.02	0.29 ± 0.08	0.32 ± 0.13				
WH2	RC _{High} :	-10.88 ± 5.06	02.63 ± 1.15	02.40 ± 1.13	03.50 ± 1.84	r = -0.8071 p = 1.51 x 10 ⁻³	r = -0.8269 p = 9.1 x 10 ⁻⁴	r = -0.8077 p = 1.5 x 10 ⁻³	r = 0.6316 p = 0.028
	RC _{Mid} :	-08.30 ± 4.34	02.09 ± 1.04	01.85 ± 0.98	02.69 ± 1.56				
	RC _{Low} :	-04.61 ± 3.11	01.26 ± 0.83	01.06 ± 0.72	01.52 ± 1.09				
	N ₂₀₀₀ :	-0.84 ± 0.30	0.19 ± 0.05	0.19 ± 0.06	0.27 ± 0.12				
	W ₂₀₁₄ :	-0.77 ± 0.24	0.17 ± 0.03	0.17 ± 0.05	0.25 ± 0.10				
Gordon River									
Flow (m ³ sec ⁻¹)	383.6 ± 38.9	360.3 ± 54.1	342.6 ± 74.6	324.3 ± 26.6	:	:	:	:	:
GAD Flow (m ³ sec ⁻¹)	107.6 ± 15.9	73.7 ± 12.1	38.8 ± 5.1	30.5 ± 2.2	:	:	:	:	:

275

Table 3: Estimated diapycnal N₂O flux (nmol N₂O m⁻² day⁻¹ ± std. dev.) calculated from local buoyancy frequencies from 20 m to 2 m within the main harbour stations. Positive values indicate the flux of N₂O from the basin water (20 m) to the surface lens (2m).

Station	July 2022 nmol N ₂ O m ⁻² day ⁻¹	October 2022 nmol N ₂ O m ⁻² day ⁻¹	February 2023 nmol N ₂ O m ⁻² day ⁻¹	April 2023 nmol N ₂ O m ⁻² day ⁻¹
KR1	80 ± 3.5	282 ± 17.7	992 ± 12.9	395 ± 8.6
C10	140 ± 4.5	1,200 ± 47.3	1,040 ± 65.3	454 ± 16.2
C08	49 ± 2.3	782 ± 12.1	778 ± 37.4	348 ± 18.6
WH2	117 ± 4.0	125 ± 2.8	1,308 ± 67.8	240 ± 18.0

Table 2).

280

Station KR1 was always observed to be a ~~net sink for atmospheric N₂O~~, ~~site of atmospheric N₂O uptake~~ and ~~was~~ every non-endmember station ~~was an estimated sink~~ in July 2022. Near the head of the system, station WH2 was observed to be a net source of N₂O to the atmosphere ~~from~~ ~~in~~ October 2022, ~~February 2023,~~ and ~~to~~ April 2023, ~~as and were~~ stations C10 and C08 (positioned above the deepest basins) ~~were net sources in~~ ~~in~~ February 2023 and April 2023.

285

Estimated diapycnal fluxes (\pm std. dev.) using local buoyancy frequencies showed a consistent upwards ~~movement of N₂O from the subhalocline to surface layers with the smallest fluxes observed in July 2022 (49 \pm 2.3 nmol N₂O m⁻² day⁻¹ at C08)~~ ~~nmol N₂O m⁻² day⁻¹ at C08)~~ and largest fluxes observed in October 2022 (up to 1308 nmol N₂O m⁻² day⁻¹ at WH2) and February 2023 (up to 1200 \pm 47.3 nmol N₂O m⁻² day⁻¹ at C10) ~~nmol N₂O m⁻² day⁻¹ at C10~~ ~~see (Table 3)~~. Patterns in the size of the diapycnal flux generally reflected the patterns of N₂O

290

Formatted: Not Highlight

Formatted: Not Highlight

Formatted: Indent: First line: 0.63 cm

Formatted: Indent: First line: 0.63 cm

Formatted: Not Highlight

Field Code Changed

% saturation with the largest fluxes occurring in October 2022 during the periods of greatest N₂O % saturation.

295 Overall the magnitude of the estimated diapycnal fluxes was smaller than estimated air/sea fluxes (~~smaller~~
~~however in February the fluxes were of similar magnitudes.~~

297

298 **Table 2:** Estimated sea-to-air N₂O flux (mean $\mu\text{mol N}_2\text{O m}^{-2} \text{ day}^{-1} \pm \text{std. dev.}$) of the main harbour stations using
 299 calculations presented in Bange et al. (2019) and Zhang et al. (2020) and a range of k_{600} parameterisations from
 300 Wanninkhof (2014; W_{2014}), Raymond and Cole (2001; RC_{Low} , RC_{Mid} , and RC_{High}), and Nightingale (2000; N_{2000}).
 301 Positive values indicate the flux of N₂O from the harbour water to the atmosphere. Negative values (shown in with
 302 bold text) indicate flux of N₂O from the atmosphere into the harbour water. Estimated Gordon River Flow and Mean
 303 (20 day) Gordon Above Dennison (GAD)Stream Gauge are also shown for each month as well as the Pearson
 304 Correlation and associated p-values between flow metrics, rainfall, and air/sea flux (and surface water % saturation).

Station	k_{600}	Jul 2022 $\mu\text{mol N}_2\text{O m}^{-2} \text{ day}^{-1}$	Oct 2022 $\mu\text{mol N}_2\text{O m}^{-2} \text{ day}^{-1}$	Feb 2023 $\mu\text{mol N}_2\text{O m}^{-2} \text{ day}^{-1}$	Apr 2023 $\mu\text{mol N}_2\text{O m}^{-2} \text{ day}^{-1}$	Gordon Flow vs Surface Flux	GAD Flow vs Surface Flux	GAD Flow vs % N ₂ O Sat.	Rainfall vs Surface Flux
KR1	RC_{High}	-11.07 ± 5.17	-04.01 ± 1.77	-03.30 ± 1.54	-03.17 ± 1.66	$r = -0.8316$ $p = 7.5 \times 10^{-4}$	$r = -0.8624$ $p = 3.1 \times 10^{-3}$	$r = -0.8726$ $p = 2.1 \times 10^{-3}$	$r = 0.5577$ $p = 0.060$
	RC_{Mid}	-08.45 ± 4.42	-03.19 ± 1.59	-02.55 ± 1.34	-02.44 ± 1.41				
	RC_{Low}	-04.69 ± 3.17	-01.93 ± 1.27	-01.46 ± 0.99	-01.38 ± 0.99				
	N_{2000}	-0.85 ± 0.31	-0.30 ± 0.08	-0.25 ± 0.09	-0.24 ± 0.11				
	W_{2014}	-0.78 ± 0.25	-0.27 ± 0.05	-0.23 ± 0.07	-0.22 ± 0.09				
C10	RC_{High}	-12.88 ± 6.00	-01.21 ± 0.53	07.31 ± 3.43	02.60 ± 1.36	$r = -0.8298$ $p = 8.4 \times 10^{-4}$	$r = -0.9091$ $p = 4.2 \times 10^{-3}$	$r = -0.8795$ $p = 1.6 \times 10^{-3}$	$r = 0.2751$ $p = 0.387$
	RC_{Mid}	-09.83 ± 5.14	-00.96 ± 0.48	05.65 ± 2.98	02.00 ± 1.16				
	RC_{Low}	-05.46 ± 3.68	-00.58 ± 0.38	03.22 ± 2.19	01.13 ± 0.81				
	N_{2000}	-0.99 ± 0.36	-0.09 ± 0.02	0.67 ± 0.23	0.20 ± 0.09				
	W_{2014}	-0.91 ± 0.29	-0.08 ± 0.02	0.61 ± 0.18	0.18 ± 0.07				
C08	RC_{High}	-03.50 ± 1.63	-01.69 ± 0.74	04.08 ± 1.91	04.57 ± 2.40	$r = -0.8547$ $p = 3.97 \times 10^{-4}$	$r = -0.8804$ $p = 1.6 \times 10^{-3}$	$r = -0.8447$ $p = 5.4 \times 10^{-4}$	$r = 0.1846$ $p = 0.566$
	RC_{Mid}	-02.67 ± 1.40	-01.34 ± 0.67	03.15 ± 1.66	03.52 ± 2.03				
	RC_{Low}	-01.49 ± 1.00	-0.81 ± 0.53	01.80 ± 1.22	01.98 ± 1.43				
	N_{2000}	-0.27 ± 0.10	-0.12 ± 0.03	0.31 ± 0.11	0.35 ± 0.15				
	W_{2014}	-0.25 ± 0.08	-0.11 ± 0.02	0.29 ± 0.08	0.32 ± 0.13				
WH2	RC_{High}	-10.88 ± 5.06	02.63 ± 1.15	02.40 ± 1.13	03.50 ± 1.84	$r = -0.8071$ $p = 1.51 \times 10^{-3}$	$r = -0.8269$ $p = 9.1 \times 10^{-4}$	$r = -0.8077$ $p = 1.5 \times 10^{-3}$	$r = 0.6316$ $p = 0.028$
	RC_{Mid}	-08.30 ± 4.34	02.09 ± 1.04	01.85 ± 0.98	02.69 ± 1.56				
	RC_{Low}	-04.61 ± 3.11	01.26 ± 0.83	01.06 ± 0.72	01.52 ± 1.09				
	N_{2000}	-0.84 ± 0.30	0.19 ± 0.05	0.19 ± 0.06	0.27 ± 0.12				
	W_{2014}	-0.77 ± 0.24	0.17 ± 0.03	0.17 ± 0.05	0.25 ± 0.10				
Gordon River Flow ($\text{m}^3 \text{sec}^{-1}$)		383.6 ± 38.9	360.3 ± 54.1	342.6 ± 74.6	324.3 ± 26.6	-	-	-	-
GAD Flow ($\text{m}^3 \text{sec}^{-1}$)		107.6 ± 15.9	73.7 ± 12.1	38.8 ± 5.1	30.5 ± 2.2	-	-	-	-

Formatted: Not Highlight

Formatted: Not Highlight

Formatted: Not Highlight

305 **Table 3:** Estimated diapycnal N₂O flux ($\text{nmol N}_2\text{O m}^{-2} \text{ day}^{-1} \pm \text{std. dev.}$) calculated from local buoyancy frequencies
 306 from 20 m to 2 m within the main harbour stations Positive values indicate the flux of N₂O from the basin water (20
 307 m) to the surface lens (2m).
 308
 309

Station	July 2022 $\text{nmol N}_2\text{O m}^{-2} \text{ day}^{-1}$	October 2022 $\text{nmol N}_2\text{O m}^{-2} \text{ day}^{-1}$	February 2023 $\text{nmol N}_2\text{O m}^{-2} \text{ day}^{-1}$	April 2023 $\text{nmol N}_2\text{O m}^{-2} \text{ day}^{-1}$
KR1	80 ± 3.5	282 ± 17.7	992 ± 12.9	395 ± 8.6
C10	140 ± 4.5	1,200 ± 47.3	1,040 ± 65.3	454 ± 16.2
C08	49 ± 2.3	782 ± 12.1	778 ± 37.4	348 ± 18.6
WH2	117 ± 4.0	125 ± 2.8	1,308 ± 67.8	240 ± 18.0

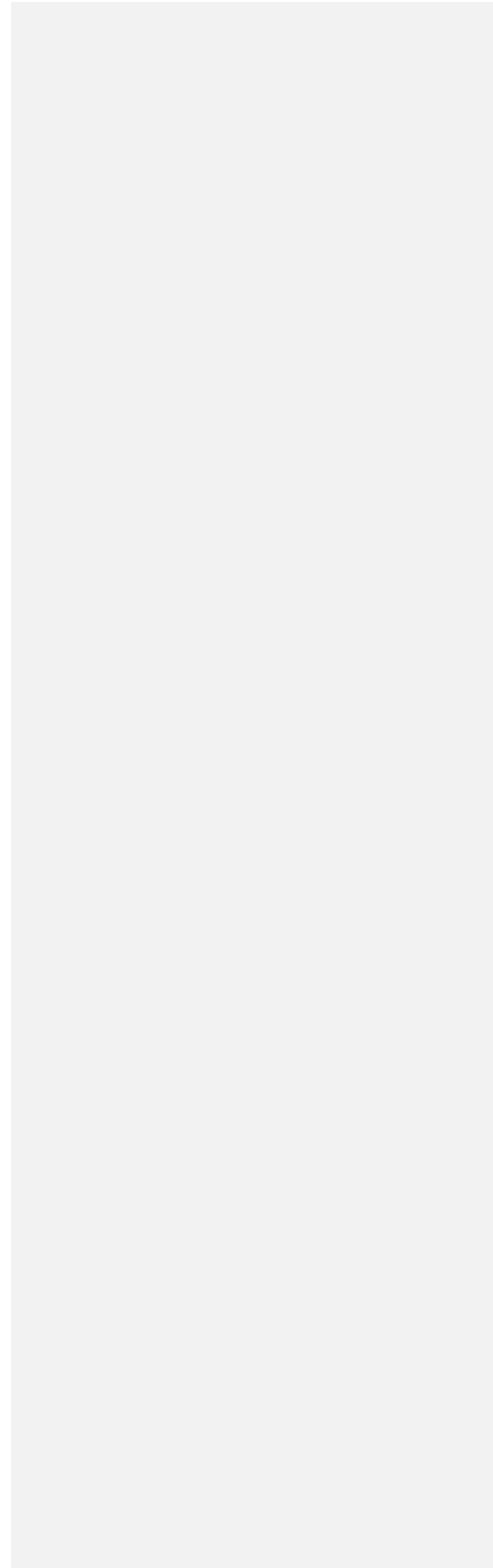
Formatted: Not Highlight

Formatted: Not Highlight

Formatted: Not Highlight

310 **Table 2:** Estimated sea-to-air N₂O flux (mean $\mu\text{mol N}_2\text{O m}^{-2} \text{ day}^{-1} \pm \text{standard error}$) of the main harbour stations
 311 using calculations presented in Bange et al. (2019) and Zhang et al. (2020) and a range of k_{600} estimators from
 312 Raymond and Cole (2001). Low, Mid, and High represent different estimators of k_{600} presented in Raymond and Cole
 313 (2001). Positive values indicate the flux of N₂O from the harbour water to the atmosphere. Negative values (shown in
 314 with bold text) indicate flux of N₂O from the atmosphere into the harbour water. Estimated Gordon River Flow and
 315 Mean (20 day) Gordon Above Dennison (GAD)Stream Gauge are also shown for each month as well as the Pearson
 316 Correlation and associated p-values between flow metrics, rainfall, and sea to air flux (and surface water %
 317 saturation).

| 319
320



321 **4. Discussion**

322 Our study is the first to report on N₂O distribution and air/sea flux from an Australasian fjord-like estuary.
 323 We set out to investigate how N₂O concentrations varied along horizontal and depth gradients; how N₂O
 324 concentrations and estimated surface water emissions vary seasonally; how N₂O concentrations vary with
 325 freshwater inputs; and whether the relationship between AOU and ΔN₂O could help clarify the primary
 326 mechanism for N₂O generation in this system.

Station	K ₆₀₀	Jul 2022 μmol N ₂ O m ⁻² day ⁻¹	Oct 2022 μmol N ₂ O m ⁻² day ⁻¹	Feb 2023 μmol N ₂ O m ⁻² day ⁻¹	Apr 2023 μmol N ₂ O m ⁻² day ⁻¹	Gordon Flow vs Surface Flux	GAD Flow vs Surface Flux	GAD Flow vs % N ₂ O Sat.	Rainfall vs Surface Flux
KR1	RC _{High} :	-11.07 ± 5.17	-04.01 ± 1.77	-03.30 ± 1.54	-03.17 ± 1.66	r = -0.8316 p = 7.5 × 10 ⁻⁴	r = -0.8624 p = 3.1 × 10 ⁻⁴	r = -0.8726 p = 2.1 × 10 ⁻⁴	r = 0.5577 p = 0.060
	RC _{Mid} :	-08.45 ± 4.42	-03.19 ± 1.59	-02.55 ± 1.34	-02.44 ± 1.41				
	RC _{Low} :	-04.69 ± 3.17	-01.93 ± 1.27	-01.46 ± 0.99	-01.38 ± 0.99				
	N ₂₀₀₀ :	-0.85 ± 0.31	-0.30 ± 0.08	-0.25 ± 0.09	-0.24 ± 0.11				
	W ₂₀₁₄ :	-0.78 ± 0.25	-0.27 ± 0.05	-0.23 ± 0.07	-0.22 ± 0.09				
C10	RC _{High} :	-12.88 ± 6.00	-01.21 ± 0.53	07.31 ± 3.43	02.60 ± 1.36	r = -0.8298 p = 8.4 × 10 ⁻⁴	r = -0.9091 p = 4.2 × 10 ⁻⁵	r = -0.8795 p = 1.6 × 10 ⁻⁴	r = 0.2751 p = 0.387
	RC _{Mid} :	-09.83 ± 5.14	-00.96 ± 0.48	05.65 ± 2.98	02.00 ± 1.16				
	RC _{Low} :	-05.46 ± 3.68	-00.58 ± 0.38	03.22 ± 2.19	01.13 ± 0.81				
	N ₂₀₀₀ :	-0.99 ± 0.36	-0.09 ± 0.02	0.67 ± 0.23	0.20 ± 0.09				
	W ₂₀₁₄ :	-0.91 ± 0.29	-0.08 ± 0.02	-0.61 ± 0.18	0.18 ± 0.07				
C08	RC _{High} :	-03.50 ± 1.63	-01.69 ± 0.74	04.08 ± 1.91	04.57 ± 2.40	r = -0.8547 p = 3.97 × 10 ⁻⁴	r = -0.8804 p = 1.6 × 10 ⁻⁴	r = -0.8447 p = 5.4 × 10 ⁻⁴	r = 0.1846 p = 0.566
	RC _{Mid} :	-02.67 ± 1.40	-01.34 ± 0.67	03.15 ± 1.66	03.52 ± 2.03				
	RC _{Low} :	-01.49 ± 1.00	-0.81 ± 0.53	01.80 ± 1.22	01.98 ± 1.43				
	N ₂₀₀₀ :	-0.27 ± 0.10	-0.12 ± 0.03	0.31 ± 0.11	0.35 ± 0.15				
	W ₂₀₁₄ :	-0.25 ± 0.08	-0.11 ± 0.02	0.29 ± 0.08	0.32 ± 0.13				
WH2	RC _{High} :	-10.88 ± 5.06	02.63 ± 1.15	02.40 ± 1.13	03.50 ± 1.84	r = -0.8071 p = 1.51 × 10 ⁻³	r = -0.8269 p = 9.1 × 10 ⁻⁴	r = -0.8077 p = 1.5 × 10 ⁻³	r = 0.6316 p = 0.028
	RC _{Mid} :	-08.30 ± 4.34	02.09 ± 1.04	01.85 ± 0.98	02.69 ± 1.56				
	RC _{Low} :	-04.61 ± 3.11	01.26 ± 0.83	01.06 ± 0.72	01.52 ± 1.09				
	N ₂₀₀₀ :	-0.84 ± 0.30	0.19 ± 0.05	0.19 ± 0.06	0.27 ± 0.12				
	W ₂₀₁₄ :	-0.77 ± 0.24	0.17 ± 0.03	0.17 ± 0.05	0.25 ± 0.10				
Gordon River Flow (m ³ sec ⁻¹)	383.6 ± 38.9	360.3 ± 54.1	342.6 ± 74.6	324.3 ± 26.6	-	-	-	-	
GAD Flow (m ³ sec ⁻¹)	107.6 ± 15.9	73.7 ± 12.1	38.8 ± 5.1	30.5 ± 2.2	-	-	-	-	

327
 328
 329 **Table 3:** Estimated diapycnal N₂O flux (nmol N₂O m⁻² day⁻¹ ± std. dev.) calculated from local buoyancy frequencies
 330 from 20 m to 2 m within the main harbour stations Positive values indicate the flux of N₂O from the basin water (20
 331 m) to the surface lens (2m).

Station	July 2022 nmol N ₂ O m ⁻² day ⁻¹	October 2022 nmol N ₂ O m ⁻² day ⁻¹	February 2023 nmol N ₂ O m ⁻² day ⁻¹	April 2023 nmol N ₂ O m ⁻² day ⁻¹
KR1	80 ± 3.5	282 ± 17.7	992 ± 12.9	395 ± 8.6
C10	140 ± 4.5	1,200 ± 47.3	1,040 ± 65.3	454 ± 16.2
C08	49 ± 2.3	782 ± 12.1	778 ± 37.4	348 ± 18.6
WH2	117 ± 4.0	125 ± 2.8	1,308 ± 67.8	240 ± 18.0

332 **Table 2.** Pearson correlations show that when freshwater flow is high N₂O air/sea flux is negative
 333 (indicating uptake from the atmosphere) and when freshwater flow is low N₂O air/sea flux is positive (**Table 2:**
 334 **Estimated sea-to-air N₂O flux (mean μmol N₂O m⁻² day⁻¹ ± std. dev.) of the main harbour stations using**
 335 **calculations presented in Bange et al. (2019) and Zhang et al. (2020) and a range of k₆₀₀ parameterisations from**
 336 **Wanninkhof (2014; W₂₀₁₄), Raymond and Cole (2001; RC_{Low}, RC_{Mid}, and RC_{High}), and Nightingale (2000; N₂₀₀₀).**

Formatted: Not Highlight

Formatted: Not Highlight

Formatted: Normal, Indent: First line: 0.63 cm

Formatted: Font: Bold, Not Highlight

Formatted: Not Highlight

Formatted: Font: Bold

Formatted: Not Highlight

337 Positive values indicate the flux of N₂O from the harbour water to the atmosphere. Negative values (shown in
 338 with bold text) indicate flux of N₂O from the atmosphere into the harbour water. Estimated Gordon River Flow
 339 and Mean (20 day) Gordon Above Dennison (GAD)Stream Gauge are also shown for each month as well as the
 340 Pearson Correlation and associated p-values between flow metrics, rainfall, and air/sea flux (and surface water %
 341 saturation).

Station	K ₆₀₀	Jul 2022 μmol N ₂ O m ⁻² day ⁻¹	Oct 2022 μmol N ₂ O m ⁻² day ⁻¹	Feb 2023 μmol N ₂ O m ⁻² day ⁻¹	Apr 2023 μmol N ₂ O m ⁻² day ⁻¹	Gordon Flow VS Surface Flux	GAD Flow VS Surface Flux	GAD Flow VS % N ₂ O Sat.	Rainfall VS Surface Flux
KR1	RC _{High} :	-11.07 ± 5.17	-04.01 ± 1.77	-03.30 ± 1.54	-03.17 ± 1.66	r = -0.8316 p = 7.5 × 10 ⁻⁴	r = -0.8624 p = 3.1 × 10 ⁻⁴	r = -0.8726 p = 2.1 × 10 ⁻⁴	r = 0.5577 p = 0.060
	RC _{Mid} :	-08.45 ± 4.42	-03.19 ± 1.59	-02.55 ± 1.34	-02.44 ± 1.41				
	RC _{Low} :	-04.69 ± 3.17	-01.93 ± 1.27	-01.46 ± 0.99	-01.38 ± 0.99				
	N ₂₀₀₀ :	-0.85 ± 0.31	-0.30 ± 0.08	-0.25 ± 0.09	-0.24 ± 0.11				
	W ₂₀₁₄ :	-0.78 ± 0.25	-0.27 ± 0.05	-0.23 ± 0.07	-0.22 ± 0.09				
C10	RC _{High} :	-12.88 ± 6.00	-01.21 ± 0.53	07.31 ± 3.43	02.60 ± 1.36	r = -0.8298 p = 8.4 × 10 ⁻⁴	r = -0.9091 p = 4.2 × 10 ⁻⁵	r = -0.8795 p = 1.6 × 10 ⁻⁴	r = 0.2751 p = 0.387
	RC _{Mid} :	-09.83 ± 5.14	-00.96 ± 0.48	05.65 ± 2.98	02.00 ± 1.16				
	RC _{Low} :	-05.46 ± 3.68	-00.58 ± 0.38	03.22 ± 2.19	01.13 ± 0.81				
	N ₂₀₀₀ :	-0.99 ± 0.36	-0.09 ± 0.02	0.67 ± 0.23	0.20 ± 0.09				
	W ₂₀₁₄ :	-0.91 ± 0.29	-0.08 ± 0.02	-0.61 ± 0.18	0.18 ± 0.07				
C08	RC _{High} :	-03.50 ± 1.63	-01.69 ± 0.74	04.08 ± 1.91	04.57 ± 2.40	r = -0.8547 p = 3.97 × 10 ⁻⁴	r = -0.8804 p = 1.6 × 10 ⁻⁴	r = -0.8447 p = 5.4 × 10 ⁻⁴	r = 0.1846 p = 0.566
	RC _{Mid} :	-02.67 ± 1.40	-01.34 ± 0.67	03.15 ± 1.66	03.52 ± 2.03				
	RC _{Low} :	-01.49 ± 1.00	-0.81 ± 0.53	01.80 ± 1.22	01.98 ± 1.43				
	N ₂₀₀₀ :	-0.27 ± 0.10	-0.12 ± 0.03	-0.31 ± 0.11	0.35 ± 0.15				
	W ₂₀₁₄ :	-0.25 ± 0.08	-0.11 ± 0.02	-0.29 ± 0.08	0.32 ± 0.13				
WH2	RC _{High} :	-10.88 ± 5.06	02.63 ± 1.15	02.40 ± 1.13	03.50 ± 1.84	r = -0.8071 p = 1.51 × 10 ⁻³	r = -0.8269 p = 9.1 × 10 ⁻⁴	r = -0.8077 p = 1.5 × 10 ⁻³	r = 0.6316 p = 0.028
	RC _{Mid} :	-08.30 ± 4.34	02.09 ± 1.04	01.85 ± 0.98	02.69 ± 1.56				
	RC _{Low} :	-04.61 ± 3.11	01.26 ± 0.83	01.06 ± 0.72	01.52 ± 1.09				
	N ₂₀₀₀ :	-0.84 ± 0.30	0.19 ± 0.05	0.19 ± 0.06	0.27 ± 0.12				
	W ₂₀₁₄ :	-0.77 ± 0.24	0.17 ± 0.03	0.17 ± 0.05	0.25 ± 0.10				
Gordon River									
Flow (m ³ sec ⁻¹)		383.6 ± 38.9	360.3 ± 54.1	342.6 ± 74.6	324.3 ± 26.6	=	=	=	=
GAD Flow (m ³ sec ⁻¹)		107.6 ± 15.9	73.7 ± 12.1	38.8 ± 5.1	30.5 ± 2.2	=	=	=	=

342
 343
 344 **Table 3: Estimated diapycnal N₂O flux (nmol N₂O m⁻² day⁻¹ ± std. dev.) calculated from local buoyancy frequencies**
 345 **from 20 m to 2 m within the main harbour stations Positive values indicate the flux of N₂O from the basin water (20**
 346 **m) to the surface lens (2m).**

Station	July 2022 nmol N ₂ O m ⁻² day ⁻¹	October 2022 nmol N ₂ O m ⁻² day ⁻¹	February 2023 nmol N ₂ O m ⁻² day ⁻¹	April 2023 nmol N ₂ O m ⁻² day ⁻¹
KR1	80 ± 3.5	282 ± 17.7	992 ± 12.9	395 ± 8.6
C10	140 ± 4.5	1,200 ± 47.3	1,040 ± 65.3	454 ± 16.2
C08	49 ± 2.3	782 ± 12.1	778 ± 37.4	348 ± 18.6
WH2	117 ± 4.0	125 ± 2.8	1,308 ± 67.8	240 ± 18.0

347 **Table 2).** Our observations highlight that freshwater flow is a key driver of N₂O emissions in this estuary. In
 348 addition, Gordon River flow is heavily influenced by hydroelectric dam release (up to ~28% of the flow in July
 349 2023). Rainfall in the catchment area may offset the effects of dam release, but our observations did not capture
 350 this as rainfall itself was not significantly correlated with N₂O concentrations or air/sea flux.

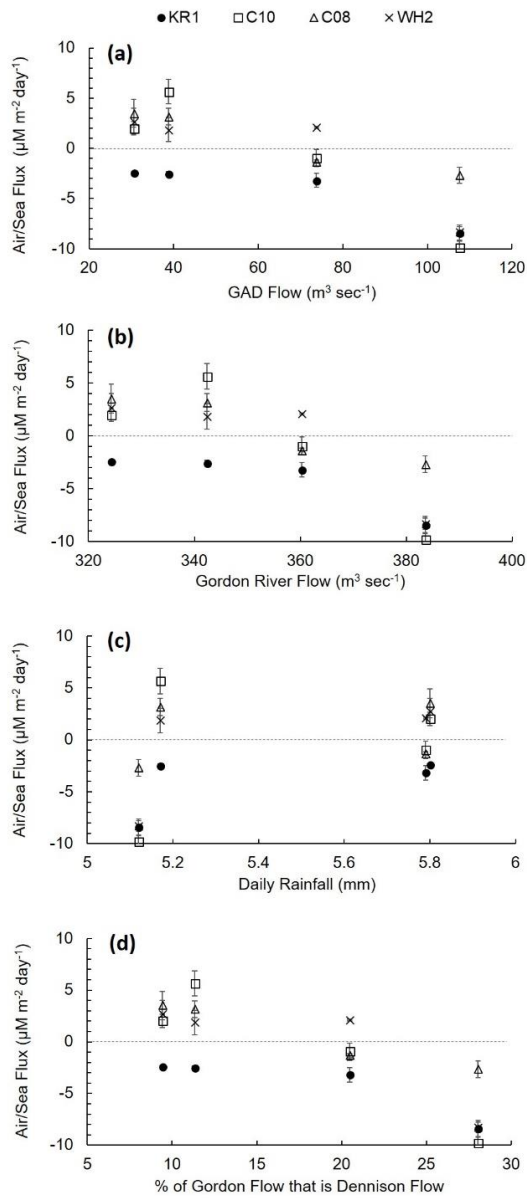
Formatted: Not Highlight

Formatted: Not Highlight

Formatted: Indent: First line: 0.63 cm

353 The river endmember concentrations of N₂O were often observed to be undersaturated, –as observed in the
354 South Platte River Basin, USA, **McMahon and Dennehy (1999)**; Neuse River Estuary, USA, **Stow et al.,**
355 **(2005)**; headwater streams, Ontario, Canada, **Baulch et al., (2011)**; and Upper Mara River Basin, Kenya,
356 **Mwanke et al., (2019)**. Our observations of endmember N₂O concentrations were similar to the lower end of the
357 concentrations reported in **McMahon and Dennehy (1999)** (approx. 80% saturation), but not as low as those
358 reported Jackson Creek, Ontario, Canada in **Baulch et al., (2011)**, whwere some observations reached <20%
359 saturation. N₂O undersaturation in those systems was attributed to complete denitrification (use of N₂O as a
360 terminal electron acceptor by denitrifies) in streams with high DOC loads, low DO, and low NO₃⁻
361 concentrations. It should also be noted that up to 28% of the estimated Gordon River flow was found to be
362 associated with flow through the Gordon Above Dennison stream gauge (a proxy for hydroelectric dam/reservoir
363 release to the Gordon River). Boreal reservoirs have been shown to be net sinks of atmospheric N₂O (**Hendzel et**
364 **al., 2005**) which was attributed to increased N₂O demand to drive complete denitrification. There is good reason
365 to believe that N₂O may be scavenged in the Gordon and King Rivers as well because they do often have high
366 DOC concentrations, high water column DO demand (**Maxey et al., 2020**), and low DO concentrations in near
367 the stream bed (**Maxey et al., 2022**).
368

Formatted: Font: Not Bold



369
 370 **Figure 68:** Mean Air/Sea Flux ($\mu\text{M m}^{-2} \text{ day}^{-1}$) versus **aA)** Gordon above Dennison River flow ($\text{m}^3 \text{ day}^{-1}$), **bB)** estimated
 371 Gordon River flow ($\text{m}^3 \text{ day}^{-1}$), **cC)** daily rainfall (mm) (20 day mean), and **dD)** % of estimated Gordon River flow this
 372 is accounted for by the Gordon above Dennison River gauge (proxy for hydroelectric dam release). Error bars
 373 indicate ± 1 standard error.

374 In the harbour's subhalocline layer there is not enough light to support photosynthesis (Hartstein *et al.*,
 375 2019; Maxey *et al.*, 2017, 2020, and 2022) and thus the main source of oxygen is advection from marine
 376 intrusions. N_2O producing microbes have been observed to populate this layer of the harbour (*see* Da Silva *et al.*,

Formatted: Superscript
 Formatted: Superscript
 Formatted: Superscript
 Formatted: Superscript
 Formatted: Superscript
 Formatted: Superscript

377 **2021 and 2022**) and our observations of supersaturated N₂O in these layers show that those microbes are active.

378 ~~The linear~~Linear relationship between AOU and ΔN₂O (slope = 0.0154; r = 0.596; p = 2.4 × 10⁻²³; **Figure 5C**~~Figure 7C~~) and NO₃⁻

379 ~~and N₂O saturation (r = 0.559; p = 6.9 × 10⁻⁹; **Figure 7D**) indicates that N₂O production likely occurs primarily~~

380 through the ammonia oxidation (nitrification) pathway (Yoshinari, 1976; Walter *et al.*, 2004; Brase *et al.*,

381 2017). Our observations are on the lower ~~end of reported N₂O yield per mole O₂ consumed end of the range reported nitrification slopes~~ (see

382 Suntharalingam and Sarmiento, 2000; Brase *et al.*, 2017) which may be an artefact of mixing and loss

383 dynamics such as basin water DO recharges from marine intrusions, and loss to aerobic respiration and the

384 atmosphere. This suggests that some portion of subhalocline pelagic oxygen demand in the harbour can be

385 ~~attributed to the oxygen demand of the fish farms. The DO concentrations in the fish farms are consistently low, and the DO~~

386 also observed similar relationships in the Saanich Inlet, a seasonally anoxic fjord-like estuary in British

387 Columbia, but in that system anoxic conditions are more persistent (Bourbonnais *et al.*, 2013; Manning *et al.*,

388 2010) compared to Macquarie Harbour (Maxey *et al.*, 2022). Deep-water renewal / marine intrusions have been

389 hypothesized to stimulate N₂O production in the Saanich Inlet (Capelle *et al.*, 2018; Michiles *et al.*, 2019; Ji *et*

390 *al.*, 2020), and Baltic Sea (Walter *et al.*, 2006) and may also be stimulating it in Macquarie Harbour as well. In

391 the Baltic Sea, Walter *et al.* (2006) and Myllykangas *et al.* (2017) observed enhanced N₂O production in areas

392 receiving significant marine intrusions. Positive correlations between AOU and ΔN₂O observed in western Baltic

393 Sea waters (Walter *et al.*, 2006) along with mean (11-year; 2006-2017) seasonal variations in DO and N₂O

394 observed through the water column at the Boknis Eck Time-Series Station (Eckernförde Bay, Southwest Baltic

395 Sea) indicate a tight coupling between DO supply and N₂O production (presumably by nitrification) /

396 consumption (presumably by denitrification) pathways in that area (Ma *et al.*, 2019). The reintroduction of

397 marine water on the upstream side of a dam in the Nakong River, South Korea was found to affect bottom water

398 trapping (stagnation), DO conditions, N process rates, process specific gene abundances, and subsequently the

399 fate of N in that system (Huang *et al.*, 2024). Marine intrusions primarily refresh the DO supply adjacent to the

400 sill in Macquarie Harbour (near station C10). As we observed a positive correlation between AOU and ΔN₂O

401 marine intrusions offer a possible explanation for the higher subhalocline N₂O concentrations observed in this

402 system. In Macquarie Harbour, the DO concentrations in the fish farms are consistently low, and the DO

403 concentrations at WH2 in October 2022 approached single digits (3.1 μM). This station has the highest basin

404 residence time compared the others used in this study. Low oxygen concentrations may also likely be found

405 under the harbour's fish farms due to the aerobic respiration of farm debris (Maxey *et al.* 2020). Though whether

406 denitrification functions as a production process or a loss process will depend upon the drivers of DO

407 concentration (*i.e.* respiration rates, physical mixing, *etc.*) and may differ depending on the location of the basins

408 in this system. It is likely the main driver of undersaturated N₂O concentrations in the Gordon River.

409

410

411 This study focusing on characterizing N₂O dynamics at end-members and at stations through the

412 harbour's longitudinal axis. Other areas of the harbour, most prominently the shallow embayments around the

413 parameter of the system and the areas occupied by fin fish farms were not included here. Fin fish aquaculture can

414 increase water column DO demand near the pens in this system (Maxey *et al.*, 2020), and introduces particulate

415 organic material to the water. Whether this manifests in altered N cycling dynamics (especially DO sensitive

416 processes like nitrification and denitrification) would be system specific and has never been described in this

Formatted: Font: Not Bold

Formatted: Font: Bold

Formatted: Not Highlight

Formatted: Not Highlight

Formatted: Not Highlight

Formatted: Font: Not Bold

Field Code Changed

Formatted: Not Highlight

Formatted: Not Highlight

Formatted: Not Highlight

417 system. High particles loads have been shown to induce denitrification in normoxic waters *e.g.* Wan et al.,
418 (2023); Frey et al., (2020); Codispoti et al., (2005); Nevison et al., (2003); Usui et al., (2001); Robinson et
419 al., (1998) so an N₂O sink might be present even under farms, even in more oxygenated basins. Future studies
420 should investigate the impacts of fin fish aquaculture on DO and N₂O cycling.

Formatted: Not Highlight

421 One source of uncertainty in our approach is in using literature derived estimators for air/sea and
422 diapycnal flux estimations. We also used literature derived k_{600} estimates from Nightingale et al., (2000),
423 Raymond and Cole (2001), and Wanninkhof (2014) to compute N₂O air/sea flux. Literature derived estimators
424 of K_{600} and eddy diffusivity are commonly used when direct measurements are unavailable (Tang et al., 2024;
425 Li et al. 2023; Murray et al. 2020) but to reduce uncertainty these are ideally measure in situ. Likewise, we
426 presented diapycnal flux estimates using turbulent eddy diffusivities from Fer et al., (2006) which were not
427 measured in Macquarie Harbour.

Formatted: Not Highlight

428 This conceptual model suggests that the harbour surface lens functions as a sink for both atmospheric
429 N₂O and N₂O generated in the subhalocline layer during high flow periods (Figure 7).

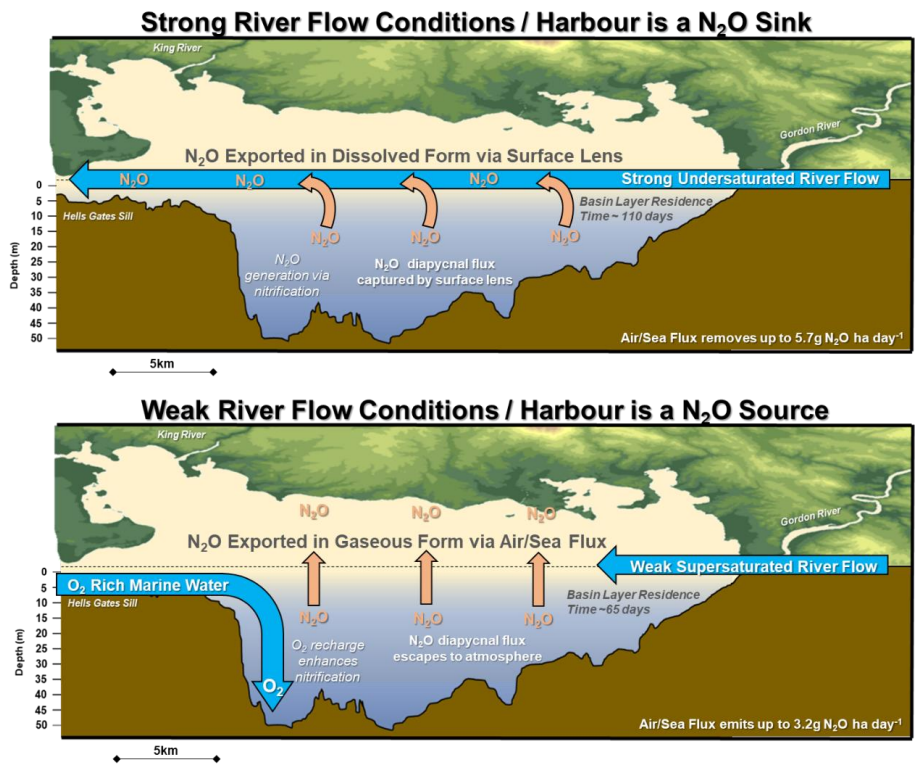
Formatted: Indent: First line: 1.27 cm

433 5. Conclusions

434 In summary, river flow, and specifically river flow driven by hydroelectric dam release, significantly affects
435 both surface water N₂O concentrations and air/sea flux in Macquarie Harbour. Importantly, when river flow is
436 low most of the harbour emits N₂O to the atmosphere. When river flow is high most of the harbour removes N₂O
437 from the atmosphere, and intercepts the diapycnal flux, and laterally exports this N₂O to the ocean in its dissolved
438 form.

Formatted: Indent: First line: 0.63 cm

439 N₂O saturation and NO₃⁻ concentration indicates that the main N₂O generation process is likely nitrification.
440 Climate change is predicted to result in wetter winter / drier summers for the Tasmanian West Coast, which may
441 result in augmented N₂O air/sea fluxes.
442 distribution, estimated air/sea flux, estimated diapycnal flux, and N₂O production pathways in this system.
443



444
 445 **Figure 79:** Conceptual model of Macquarie Harbour's N₂O dynamics. The top diagram depicts the capture of N₂O
 446 generated in the subhalocline during strong river flow conditions. Here N₂O is exported from the harbour in its
 447 dissolved form via undersaturated surface flows from the harbour to the ocean. The bottom diagram depicts the
 448 efflux of N₂O from the harbour surface during low flow conditions. Note that during these conditions the surface
 449 flows are weak and generally supersaturated with N₂O permitting its escape in gaseous form to the atmosphere.

450

451 **6. Appendix**

452 **Table A1: N₂O fluxes and observed ranges of mean (± standard deviation) N₂O concentration / saturation from both**
 453 **fjord-like / river dominated estuaries around the globe and estuaries in Australia.**

Location	System Type	Measurement Depth Range	Mean Sea-to-Air N ₂ O flux uMol N ₂ O m ⁻² day ⁻¹	Min and Max Sea-to-Air N ₂ O flux uMol N ₂ O m ⁻² day ⁻¹	Mean N ₂ O Concentration (and Saturation) nM N ₂ O (and %)	Min and Max N ₂ O Concentration (and Saturation) nM N ₂ O (and %)	Reference
Macquarie Harbour, Western Tasmania, Australia	Fjord-like Estuary	2m to 45m	-09.83 ± 0.67 to 05.65 ± 1.22	-10.82 to 7.73	11.7 ± 1.6 (121.8 ± 17.8)	7.87 to 17.12 (81 to 174)	<i>This Study</i>
Reloncaví Estuary, Chile	Fjord-like Estuary	0m to 5m	0.86 ± 2.28	-1.58 to 5.60	11.8 ± 1.70 (111 ± 18.3)	8.34 to 14.5 (80 to 140)	Yevenes <i>et al.</i> , 2017
Reloncaví Estuary, Chile	Fjord-like Estuary	10m to 200m	-	-	14.5 ± 1.73 (145 ± 17.7)	10.5 to 17.0 (11 to 170)	Yevenes <i>et al.</i> , 2017
Chiloé Interior Sea, Chile	Fjord-like Estuary	0m to 200m	1.08 ± 1.41	-0.18 to 3.19	12.6 ± 2.36 (121 ± 17.5)	8.81 to 21.1 (87 to 160)	Yevenes <i>et al.</i> , 2017
Europa Sound, Magellanic Region, Chile	Fjord-like Estuary	1m to 10m	-15.22 to -0.81	-	11.9 ± 5.7 to 12.7 ± 1.0	-	Fariás <i>et al.</i> , 2018
Concepción Channel, Magellanic Region, Chile	Fjord-like Estuary	1m to 150m	0.69 to 7.70	-	13.6 ± 1.1 to 17.0 ± 0.02	-	Fariás <i>et al.</i> , 2018
Sarmiento Channel, Magellanic Region, Chile	Fjord-like Estuary	1m to 10m	2.07 to 12.53	-	13.1 ± 0.1 to 16.5 ± 0.3	-	Fariás <i>et al.</i> , 2018
Estero Peel, Magellanic Region, Chile	Fjord-like Estuary	1m to 10m	0.11 to 2.01	-	13.1 ± 0.2 to 13.5 ± 0.5	-	Fariás <i>et al.</i> , 2018
Estero Calvo, Magellanic Region, Chile	Fjord-like Estuary	1m to 10m	0.04	-	13.9 ± 0.8	-	Fariás <i>et al.</i> , 2018
Estero Amalia, Magellanic Region, Chile	Fjord-like Estuary	1m to 100m	-0.08	-	14.2 ± 1.7	-	Fariás <i>et al.</i> , 2018
Estero las Montañas, Magellanic Region, Chile	Fjord-like Estuary	1m to 10m	-2.95	-	9.69 ± 1.6	-	Fariás <i>et al.</i> , 2018
Smyth Channel, Magellanic Region, Chile	Fjord-like Estuary	1m to 300m	1.07 to 11.2	-	14.3 ± 0.4 to 16.0 ± 0.5	-	Fariás <i>et al.</i> , 2018
Última Esperanza Sound, Magellanic Region, Chile	Fjord-like Estuary	1m to 10m	-3.7 to 10.4	-	12.1 ± 1.1 to 13.7 ± 0.07	-	Fariás <i>et al.</i> , 2018
Almirante Mott Gulf, Magellanic Region, Chile	Fjord-like Estuary	1m to 150m	15.6	-	21.0 ± 5.7	-	Fariás <i>et al.</i> , 2018
Kirke Channel, Magellanic Region, Chile	Fjord-like Estuary	1m to 10m	0.12 to 8.19	-	13.3 ± 0.1 to 15.4 ± 0.4	-	Fariás <i>et al.</i> , 2018
Union Channel, Magellanic Region, Chile	Fjord-like Estuary	1m to 10m	22.1	-	16.7 ± 0.8	-	Fariás <i>et al.</i> , 2018
Union Sound, Magellanic Region, Chile	Fjord-like Estuary	1m to 10m	2.86	-	14.8 ± 0.8	-	Fariás <i>et al.</i> , 2018
Western Magellan Strait, Magellanic Region, Chile	Fjord-like Estuary	1m to 10m	143	-	15.71	-	Fariás <i>et al.</i> , 2018
Eastern Magellan Strait, Magellanic Region, Chile	Fjord-like Estuary	1m	36.3	-	16.4	-	Fariás <i>et al.</i> , 2018
San Gregorio Cape, Magellanic Region, Chile	Fjord-like Estuary	1m	24.8	-	12.07	-	Fariás <i>et al.</i> , 2018
Otway Center Sound, Magellanic Region, Chile	Fjord-like Estuary	1m	35.5	-	11.4	-	Fariás <i>et al.</i> , 2018
Magdalena North Channel, Magellanic Region, Chile	Fjord-like Estuary	1m	-0.22	-	11.4	-	Fariás <i>et al.</i> , 2018
Chasco Sound, Magellanic Region, Chile	Fjord-like Estuary	1m	6.81	-	16.01	-	Fariás <i>et al.</i> , 2018
Cockburn West Channel, Magellanic Region, Chile	Fjord-like Estuary	1m	6.18	-	14.47	-	Fariás <i>et al.</i> , 2018
Saanich Inlet, British Columbia, Canada	Fjord-like Estuary	10m to 200m	2.3 ± 2.5 to 3.9 ± 2.9	-	14.7	<0.5 to 37.4	Capelle <i>et al.</i> , 2018
Saanich Inlet, British Columbia, Canada	Fjord-like Estuary	Surface to 110m	11.3 to 20.4	-	-	-	Cohen 1978
Elbe River Estuary, Germany	Well-Mixed River Dominated Estuary	1.2m	-	26.0 ± 23.5 to 100.7 ± 101.2	-	(161 ± 53.6) to (243 ± 141.6)	Schulz <i>et al.</i> 2023
Eckernförde Bay, Boknis Eck Time Series Station, Baltic Sea, Germany	Enclosed Sea	1m to 25m	3.5 ± 12.4	-19.0 to 105.7	(111 ± 30)	(56 to 314)	Ma <i>et al.</i> , 2019
Eckernförde Bay, Boknis Eck Time Series Station, Baltic Sea, Germany	Enclosed Sea	1m to 25m	-	-	10 to 17	-	Walter <i>et al.</i> , 2006
Baltic Sea, Germany	Enclosed Sea	110m	5 -11	-	14 to 1523	-	Rönner 1983

Gotland Basin, Baltic Sea, Germany	Enclosed Sea	90m	-	-	13	0 to 126 (0 to 450)	Brettar and Rheinheimer 1991
Northwest Shelf, Black Sea	Enclosed Sea	-	1.6 to 4.4	-	6.5 to 8	-	Amouroux <i>et al.</i> , 2002
Deep Basin, Black Sea	Enclosed Sea	70m	3.1 to 5.2	-	7.5 to 10.2	-	Amouroux <i>et al.</i> , 2002
Cariaco Basin, Venezuela	Coastal Basin	Surface to 400m	-	-	4.4 to 5.5	-	Hashimoto <i>et al.</i> , 1983
Guadalquivir Estuary, Gulf of Cadiz, Spain	River Dominated Estuary	2m	18.7 ± 33.6	-	20.6 ± 24.3	-	Sierra <i>et al.</i> , 2020
Guadalquivir Estuary, Gulf of Cadiz, Spain	River Dominated Estuary	2m	0.3 ± 0.5	-	6.7 ± 0.4	-	Sierra <i>et al.</i> , 2020
Guadalquivir Estuary, Gulf of Cadiz, Spain	River Dominated Estuary	2m	0.9 ± 21.6	-	7.3 ± 15.4	-	Sierra <i>et al.</i> , 2020
Noosa River Estuary, Eastern Australia	River Dominated Estuary	0.5m to 9.6m	-14.24 ± 14.02	-57.72 to 22.20	6.99 ± 0.43 (97 ± 2.2)	5.92 to 7.95 (90 to 103)	Wells <i>et al.</i> , 2018
Mooloolah River Estuary, Eastern Australia	River Dominated Estuary	0.5m to 6.8m	-7.33 ± 7.25	-48.76 to 16.31	6.74 ± 0.64 (97 ± 3.8)	5.19 to 7.71 (82 to 112)	Wells <i>et al.</i> , 2018
Maroochy River Estuary, Eastern Australia	River Dominated Estuary	0.5m to 8.2m	51.33 ± 55.3	-34.94 to 179.64	8.4 ± 1.50 (113 ± 16.7)	6.07 to 12.93 (92 to 163)	Wells <i>et al.</i> , 2018
Pine River Estuary, Eastern Australia	River Dominated Estuary	0.5m to 10.1m	17.10 ± 39.44	-33.22 to 145.50	7.1 ± 0.76 (102 ± 6.24)	6.05 to 8.57 (93 to 117)	Wells <i>et al.</i> , 2018
Brisbane River Estuary, Eastern Australia	River Dominated Estuary	0.5m to 23.9m	209.54 ± 143.59	15.42 to 662.62	9.8 ± 1.36 (133 ± 9.9)	6.75 to 12.75 (105 to 158)	Wells <i>et al.</i> , 2018
Middle Reach, Brisbane River Estuary, Eastern Australia	River Dominated Estuary	Surface	14.5 ± 1.19	5.4 ± 0.34 to 25.2 ± 1.87	-	13.1 to 17.9 (160 to 250)	Sturm <i>et al.</i> , 2017
Lower Reach, Brisbane River Estuary, Eastern Australia	River Dominated Estuary	Surface	6. ± 0.51	3.7 ± 0.85 to 9.1 ± 1.19	-	9.2 to 12.7 (125 to 410)	Sturm <i>et al.</i> , 2017
Oxley Creek, Eastern Australia	River Dominated Estuary	2.1m to 13.1m	210.59 ± 60.23	91.54 to 280.16	11.7 ± 1.34 (156 ± 19.7)	9.65 to 14.89 (139 to 199.7)	Wells <i>et al.</i> , 2017
Nerang River Estuary, Eastern Australia	River Dominated Estuary	0.5m to 6.8m	-0.62 ± 20.87	-67.98 to 45.92	6.73 ± 0.43 (100 ± 4.3)	5.99 to 7.79 (88 to 109)	Wells <i>et al.</i> , 2018
Logan River Estuary, Eastern Australia	-	0.5m to 14.4m	110.00 ± 153.55	-54.48 to 796.00	9.3 ± 2.36 (127 ± 27.5)	5.54 to 14.8 (81 to 191)	Wells <i>et al.</i> , 2018
Albert River Estuary, Eastern Australia	-	1.1m to 15.7m	90.05 ± 73.32	-9.50 to 264.25	10.10 ± 2.24 (131 ± 29.8)	7.32 to 15.1 (98 to 205)	Wells <i>et al.</i> , 2018
Darwin Creek, Australia	Mangrove Creek	~1m	-0.12	-	6.3 (98.9)	6.0 to 6.8 (95 to 104)	Maher <i>et al.</i> , 2016
Hinchinbrook Creek, Australia	Mangrove Creek	~1m	-3.43	-	6.1 (83.3)	5.6 to 6.8 (75 to 91)	Maher <i>et al.</i> , 2016
Melbourne Creek, Australia	Mangrove Creek	~1m	-1.33	-	7.9 (96.6)	6.9 to 9.1 (86 to 115)	Maher <i>et al.</i> , 2016
Morton Bay Creek, Australia	Mangrove Creek	~1m	-3.19	-	5.1 (77.4)	3.4 to 6.6 (50 to 105)	Maher <i>et al.</i> , 2016
Seventeen Seventy Creek, Australia	Mangrove Creek	~1m	-1.75	-	7.7 (94.3)	7.1 to 8.9 (88 to 106)	Maher <i>et al.</i> , 2016
Brisbane River, Australia	-	-	-	-	(285)	(135 to 435)	Musenze <i>et al.</i> , 2014
Coffs Creek, Australia	-	-	-	-	(219 ± 37)	(53 to 386)	Reading <i>et al.</i> , 2017
Coffs Creek, Australia	-	-	-	-	(266.5 ± 128)	(86 to 678)	Reading <i>et al.</i> , 2020
Boambee Creek, Australia	-	-	-	-	(197.1 ± 75)	(87 to 329)	Reading <i>et al.</i> , 2020
Bonville Creek, Australia	-	-	-	-	(183.7 ± 65)	(78 to 310)	Reading <i>et al.</i> , 2020
Pine Creek, Australia	-	-	-	-	(194.1 ± 65)	(79 to 382)	Reading <i>et al.</i> , 2020
Yarra River, Australia	Salt Wedge Estuary	-	-	-	(135.9 ± 31)	-	Tait <i>et al.</i> , 2017

454 **7. Acknowledgments**

455 We would like to thank GEOMAR for providing the facilities and training (thank you Lea, Florian, and
456 Chukwudi) required to analyse N₂O samples. We want to thank Torsten and Leonie Schwoch for their sampling
457 assistance and tireless vessel operation on the Harbour. We want to thank the ADS Environmental Services *Sdn.*
458 *Bhd.* technical staff for helping to collect portions of this dataset (Grace, Shukry, Atika, Chance, Gene, and
459 Azza). We would also like to thank our families for supporting our long days away from home.

460
461 This research has been supported by internal funding from ADS Environmental Services, Swinburne University
462 of Technology student travel grant, and GEOMAR.

463
464 We have used some of the data available in the MEMENTO database. The MEMENTO database is administered
465 by the Kiel Data Management Team at GEOMAR Helmholtz Centre for Ocean Research Kiel. The database is
466 accessible through the MEMENTO webpage: <https://memento.geomar.de>.

467 **8. Data Availability**

468 This data set is available upon request

469 **9. Author Contributions**

470 **Johnathan Daniel Maxey** – *Conceptualization, Field Collection, Analytical Methodology, Data*
471 *Analysis, Writing – Original Draft, Writing – Review & Editing*

472

473 **Neil David Hartstein** – *Conceptualization, Field Collection, Analytical Guidance, Writing – Review &*
474 *Editing, Funding*

475

476 **Hermann W. Bange** – *Conceptualization, Analytical Methodology, Data Analysis, Writing – Review*
477 *& Editing*

478

479 **Moritz Müller** – *Conceptualization, Field Collection, Analytical Guidance, Writing – Review &*
480 *Editing*

481

482 **10. Competing Interests**

483 HWB serves on the editorial board for Biogeosciences. The authors declare that they have no other conflicts of
484 interest.

485

486 **11. References**

487 [Borges, A. V., Delille, B., Schiettecatte, L. S., Gazeau, F., Abril, G., and Frankignoulle, M.: Gas transfer](#)
488 [velocities of CO₂ in three European estuaries \(Randers Fjord, Scheldt, and Thames\). *Limnology and*](#)
489 [Oceanography, 49\(5\), 1630-1641, 2004. DOI: 10.4319/lo.2004.49.5.1630](#)

490

491 [Acuña-González, J. A., Vargas-Zamora, J. A., and Córdoba-Muñoz, R.: A snapshot view of some vertical](#)
492 [distributions of water parameters at a deep \(200 m\) station in the fjord-like Golfo Dulce, embayment, Costa Rica.](#)
493 [Revista de Biología Tropical, 54\(1\), 193-200, 2006. ISSN: 0034-7744](#)

494

495 [Amouroux, D., Roberts, G., Rapsomanikis, S., and Andreae, M. O.: Biogenic gas \(CH₄, N₂O, DMS\) emission to](#)
496 [the atmosphere from near-shore and shelf waters of the north-western Black Sea. *Estuarine, Coastal and Shelf*](#)
497 [Science, 54\(3\), 575-587, 2002. DOI: 10.1006/ecss.2000.0666](#)

498

499 [Andrewartha, J. and Wild-Allen, K.: CSIRO Macquarie Harbour Hydrodynamic and Oxygen Tracer Modelling.](#)
500 [Progress report to FRDC 2016/067 Project Steering Committee, 2017.](#)
501
502 [Arneborg, L., Janzen, C., Liljebladh, B., Rippeth, T. P., Simpson, J. H., and Stigebrandt, A.: Spatial variability of](#)
503 [diapycnal mixing and turbulent dissipation rates in a stagnant fjord basin. Journal of Physical Oceanography,](#)
504 [34\(7\), 1679-1691, 2004. DOI: 10.1175/1520-0485\(2004\)034<1679:SVODMA>2.0.CO;2](#)
505
506 [Austin, W. E., and Inall, M. E.: Deep-water renewal in a Scottish fjord: temperature, salinity and oxygen](#)
507 [isotopes. Polar Research, 21\(2\), 251-257, 2002. DOI: 10.3402/polar.v21i2.6485](#)
508
509 [Bange, H. W., Rapsomanikis, S., and Andreae, M. O.: Nitrous oxide in coastal waters. Global Biogeochemical](#)
510 [Cycles, 10\(1\), 197-207, 1996. DOI: 10.1029/95GB03834.](#)
511
512 [Bange, H. W.: Nitrous oxide and methane in European coastal waters. Estuarine, Coastal and Shelf Science,](#)
513 [70\(3\), 361-374, 2006. DOI: 10.1016/j.ecss.2006.05.042](#)
514
515 [Bange, H. W., Bell, T. G., Comejo, M., Freing, A., Uher, G., Upstill-Goddard, R. C., and Zhang, G. L.:](#)
516 [MEMENTO: A proposal to develop a database of marine nitrous oxide and methane measurements.](#)
517 [Environmental Chemistry, 6, 195-197, 2009. DOI: 10.1071/en09033.](#)
518
519 [Bange, H. W., Sim, C. H., Bastian, D., Kallert, J., Kock, A., Mujahid, A., and Müller, M.: Nitrous oxide \(N₂O\)](#)
520 [and methane \(CH₄\) in rivers and estuaries of northwestern Borneo. Biogeosciences, 16\(22\), 4321-4335, 2019.](#)
521 [DOI: 10.5194/bg-16-4321-2019](#)
522
523 [Bange, H. W., Mongwe, P., Shutler, J. D., Arévalo-Martínez, D. L., Bianchi, D., Lauvset, S. K., Liu, C., Löscher,](#)
524 [C. R., Martins, H., Rosentreter, J. A., Schmale, O., Steinhoff, T., Upstill-Goddard, R. C., Wanninkhof, R.,](#)
525 [Wilson, S. T., and Xie, H.: Advances in understanding of air–sea exchange and cycling of greenhouse gases in](#)
526 [the upper ocean, Elementa: Science of the Anthropocene, 12, 2024. DOI: 10.1525/elementa.2023.00044](#)
527
528 [Bastian, D.: N₂O und CH₄ Verteilung in Ästuaren und Flüssen im Nordwesten von Borneo, 2017. BSc thesis,](#)
529 [Kiel University, Kiel, 50 pp., 2017.](#)
530
531 [Baulch, H. M., Schiff, S. L., Maranger, R., and Dillon, P. J.: Nitrogen enrichment and the emission of nitrous](#)
532 [oxide from streams. Global Biogeochemical Cycles, 25\(4\), 2011. DOI: 10.1029/2011GB004047](#)
533
534 [Beaulieu, J. J., Shuster, W. D., and Rebolz, J. A.: Controls on gas transfer velocities in a large river. Journal of](#)
535 [Geophysical Research: Biogeosciences, 117\(G2\), 2012. DOI: 10.1029/2011JG001794](#)
536
537 [Bennett, J. C., Ling, F. L. N., Graham, B., Grose, M. R., Corney, S. P., White, C. J., Holz, G. K., Post, D. A.,](#)
538 [Gaynor, S. M. and Bindoff, N. L.: Climate Futures for Tasmania: water and catchments technical report.](#)

539 [Antarctic Climate & Ecosystems Cooperative Research Centre, Hobart, Tasmania, 2010. ISBN: 978-1-921197-](#)
540 [06-8](#)
541
542 [Bianchi, T. S., Cui, X., Blair, N. E., Burdige, D. J., Eglinton, T. I., and Galy, V.: Centers of organic carbon burial](#)
543 [and oxidation at the land-ocean interface. Organic Geochemistry, 115, 138-155, 2018. DOI:](#)
544 [10.1016/j.orggeochem.2017.09.008](#)
545
546 [Bianchi, T. S., Arndt, S., Austin, W. E., Benn, D. I., Bertrand, S., Cui, X., Faust, J., Koziarowska-Makuch, K.,](#)
547 [Moy, C., Savage, C., Smeaton, C., Smith, R., and Syvitski, J.: Fjords as aquatic critical zones \(ACZs\). Earth-](#)
548 [Science Reviews, 203\(103145\), 2020. DOI: 10.1016/j.earscirev.2020.103145](#)
549
550 [Brase, L., Bange, H. W., Lendt, R., Sanders, T., and Dähnke, K.: High resolution measurements of nitrous oxide](#)
551 [\(N₂O\) in the Elbe estuary. Frontiers in Marine Science, 4\(162\), 2017. DOI: 10.3389/fmars.2017.00162](#)
552
553 [Breider, F., Yoshikawa, C., Makabe, A., Toyoda, S., Wakita, M., Matsui, Y., Kawagucci, S., Fujiki, T., Harada,](#)
554 [N. and Yoshida, N.: Response of N₂O production rate to ocean acidification in the western North Pacific. Nature](#)
555 [Climate Change, 9\(12\), 954-958, 2019. DOI: 10.1038/s41558-019-0605-7](#)
556
557 [Breitburg, D., Grégoire, M., and Isensee, K. \(eds\): Global Ocean Oxygen Network 2018. The ocean is losing its](#)
558 [breath: Declining oxygen in the world's ocean and coastal waters. OC-UNESCO, IOC Technical Series, No. 137,](#)
559 [2018.](#)
560
561 [Brettar, I., and Rheinheimer, G.: Denitrification in the Central Baltic: evidence for H₂S-oxidation as motor of](#)
562 [denitrification at the oxic-anoxic interface. Marine Ecology Progress Series, 77\(2-3\), 157-169, 1991.](#)
563 [http://www.jstor.org/stable/24826569](#)
564
565 [Bourbonnais, A., Lehmann, M. F., Hamme, R. C., Manning, C. C., and Juniper, S. K.: Nitrate elimination and](#)
566 [regeneration as evidenced by dissolved inorganic nitrogen isotopes in Saanich Inlet, a seasonally anoxic fjord.](#)
567 [Marine Chemistry, 157, 194-207, 2013. DOI: 10.1016/j.marchem.2013.09.006](#)
568
569 [Capelle, D. W., Hawley, A. K., Hallam, S. J., and Tortell, P. D.: A multi-year time-series of N₂O dynamics in a](#)
570 [seasonally anoxic fjord: Saanich Inlet, British Columbia. Limnology and Oceanography, 63\(2\), 524-539, 2018.](#)
571 [DOI: 10.1002/lno.10645](#)
572
573 [Carpenter, P. D., Butler, E. C. V., Higgins, H. W., Mackey, D. J., and Nichols, P. D.: Chemistry of trace](#)
574 [elements, humic substances and sedimentary organic matter in Macquarie Harbour, Tasmania. Marine and](#)
575 [Freshwater Research, 42\(6\), 625-654, 1991. DOI: 10.1071/MF9910625](#)
576

577 [Chen, C., Pan, J., Xiao, S., Wang, J., Gong, X., Yin, G., Hou, L., Liu, M., and Zheng, Y.: Microplastics alter](#)
578 [nitrous oxide production and pathways through affecting microbiome in estuarine sediments. *Water Research*](#)
579 [221\(118733\), 2022. DOI: 10.1016/j.watres.2022.118733](#)

580

581 [Chen, J., Wells, N. S., Erler, D. V., and Eyre, B. D.: Land-use intensity increases benthic N₂O emissions across](#)
582 [three sub-tropical estuaries. *Journal of Geophysical Research: Biogeosciences* 127, 2022. DOI:](#)
583 [10.1029/2022JG006899](#)

584

585 [Cresswell, G. R., Edwards, R. J., Barker, B. A.: Macquarie Harbour, Tasmania-seasonal oceanographic](#)
586 [surveys in 1985. University of Tasmania Journal contribution. 1989. DOI: 10.26749/rstpp.123.63](#)

587

588 [de Bie, M. J. M.: Factors controlling nitrification and nitrous oxide production in the Schelde estuary. Doctoral](#)
589 [dissertation, Yerseke: Netherlands Institute of Ecology \(NIOO-CEMO\). 2002.](#)

590

591 [Dey, R., Lewis, S. C., Arblaster, J. M., and Abram, N. J.: A review of past and projected changes in Australia's](#)
592 [rainfall. *Wiley Interdisciplinary Reviews: Climate Change*, 10\(3\), e577, 2019. DOI: 10.1002/wcc.577](#)

593

594 [Etminan, M., Myhre, G., Highwood, E. J., and Shine, K. P.: Radiative forcing of carbon dioxide, methane, and](#)
595 [nitrous oxide: A significant revision of the methane radiative forcing. *Geophysical Research Letters*, 43\(24\), 12-](#)
596 [614, 2016. DOI: 10.1002/2016GL071930](#)

597

598 [Eyring, V., Gillett, N. P., Achuta Rao, K. M., Barimalala, R., Barreiro Parrillo, M., Bellouin, N., Cassou, C.,](#)
599 [Durack, P. J., Kosaka, Y., McGregor, S., Min, S., Morgenstern, O., Sun, Y.: Human Influence on the Climate](#)
600 [System. In *Climate Change 2021: The Physical Science Basis. Contribution of Working Group I to the Sixth*](#)
601 [Assessment Report of the Intergovernmental Panel on Climate Change. Masson-Delmotte, V., Zhai, P., Pirani,](#)
602 [A., Connors, S. L., Péan, C., Berger, S., Caud, N., Chen, Y., Goldfarb, L., Gomis, M. I., Huang, M., Leitzell,](#)
603 [K., Lonnoy, E., Matthews, J. B. R., Maycock, T. K., Waterfield, T., Yelekçi, O., Yu, R., and Zhou, B. \(eds.\):](#)
604 [Cambridge University Press, Cambridge, United Kingdom and New York, NY, USA, 423–552, 2021. DOI:](#)
605 [10.1017/9781009157896.005.](#)

606

607 [Farias, L., Bello, E., Arancibia, G., Fernandez, J.: Distribution of dissolved methane and nitrous oxide in Chilean](#)
608 [coastal systems of the Magellanic Sub-Antarctic region \(50°–55°S\). *Estuarine, Coastal and Shelf Science*, 215,](#)
609 [225-240, 2018. DOI: 10.1016/j.ecss.2018.10.020.](#)

610

611 [Fer, I.: Scaling turbulent dissipation in an Arctic fjord. *Deep Sea Research Part II: Topical Studies in*](#)
612 [Oceanography, 53\(1-2\), 77-95, 2006. DOI: 10.1016/j.dsr2.2006.01.003](#)

613

614 [Forster P., Storelvmo T., Armour K., Collins W., Dufresne J.-L., Frame D., Lunt, D., Mauritsen, T., Palmer, M.,](#)
615 [Watanabe, M., Wild, M.: The earth's energy budget, climate feedbacks, and climate sensitivity In *Climate*](#)
616 [Change 2021: The Physical Science Basis. Contribution of Working Group I to the Sixth Assessment Report of](#)

617 [the Intergovernmental Panel on Climate Change. Masson-Delmotte, V., Zhai, P., Pirani, A., Connors, S. L.,](#)
618 [Péan, C., Berger, S., Caud, N., Chen, Y., Goldfarb, L., Gomis, M. I., Huang, M., Leitzell, K., Lonnoy, E.,](#)
619 [Matthews, J. B. R., Maycock, T. K., Waterfield, T., Yelekçi, O., Yu, R., and Zhou, B. \(eds.\): Cambridge](#)
620 [University Press, Cambridge, United Kingdom and New York, NY, USA, 423–552, 2021. DOI:](#)
621 [10.1017/9781009157896.009](#)

622

623 [Gilbert, D., Rabalais, N. N., Diaz, R. J., & Zhang, J.: Evidence for greater oxygen decline rates in the coastal](#)
624 [ocean than in the open ocean. *Biogeosciences*, 7\(7\), 2283-2296, 2010. DOI: 10.5194/bg-7-2283-2010](#)

625

626 [Gillibrand, P. A., Cage, A. G., and Austin, W. E. N.: A preliminary investigation of basin water response to](#)
627 [climate forcing in a Scottish fjord: evaluating the influence of the NAO. *Continental Shelf Research*, 25\(5-6\),](#)
628 [571-587, 2005. DOI: 10.1016/j.csr.2004.10.011](#)

629

630 [Grose, M. R., Barnes-Keoghan, I., Corney S. P., White C. J., Holz, G.K., Bennett, J. B., Gaynor, S.M. and](#)
631 [Bindof, N.L.: Climate Futures for Tasmania: general climate impacts technical report. Antarctic Climate &](#)
632 [Ecosystems Cooperative Research Centre, Hobart, Tasmania, 2010. ISBN: 978-1-921197-05-5](#)

633

634 [Hartstein, N. D., Maxey, J. D., Loo, J. C. H., and Then, A. Y. H.: Drivers of deep water renewal in Macquarie](#)
635 [Harbour, Tasmania. *Journal of Marine Systems*, 199\(103226\), 2019. DOI: 10.1016/j.jmarsys.2019.103226](#)

636

637 [Hashimoto, L. K., Kaplan, W. A., Wofsy, S. C., and McElroy, M. B.: Transformations of fixed nitrogen and](#)
638 [N₂O in the Cariaco Trench. *Deep Sea Research Part A. Oceanographic Research Papers*, 30\(6\), 575-590, 1983.](#)
639 [DOI: 10.1016/0198-0149\(83\)90037-7](#)

640

641 [Hendzel, L. L., Matthews, C. J. D., Venkiteswaran, J. J., St. Louis, V. L., Burton, D., Joyce, E. M., and Bodaly,](#)
642 [R. A.: Nitrous oxide fluxes in three experimental boreal forest reservoirs. *Environmental Science & Technology*,](#)
643 [39\(12\), 4353-4360, 2005. DOI: 10.1021/es049443j](#)

644

645 [Huang, Y., Song, B., Zhang, Q., Park, Y., Wilson, S. J., Tobias, C. R., and An, S.: Seawater intrusion effects on](#)
646 [nitrogen cycling in the regulated Nakdong River Estuary, South Korea. *Frontiers in Marine Science*,](#)
647 [11\(1369421\), 2024. DOI: 10.3389/fmars.2024.1369421](#)

648

649 [Inall, M. E., & Gillibrand, P. A.: The physics of mid-latitude fjords: a review. *Geological Society, London,*](#)
650 [Special Publications, 344\(1\), 17-33, 2010. DOI: 10.1144/SP344.3](#)

651

652 [Ji, Q., Jameson, B. D., Juniper, S. K., and Grundle, D. S.: Temporal and vertical oxygen gradients modulate](#)
653 [nitrous oxide production in a seasonally anoxic fjord: Saanich Inlet, British Columbia. *Journal of Geophysical*](#)
654 [Research: Biogeosciences, 125\(9\), 2020. DOI: 10.1029/2020JG005631](#)

655

656 [Kallert, J.: Verteilung von Lachgas \(N₂O\) und Methan \(CH₄\) im Fluss Rajang \(Malaysia\). Bachelor thesis,](#)
657 [Christian-Albrecht-University, Kiel, 2017. URI: https://oceanrep.geomar.de/id/eprint/40913/](#)
658
659 [Kock, A. and Bange, H. W.: Counting the ocean's greenhouse gas emissions. *Eos: Earth & Space Science News*,](#)
660 [96\(3\), 10–13, 2015. DOI:10.1029/2015EO023665](#)
661
662 [Ku, Harry H. "Notes on the use of propagation of error formulas." *Journal of Research of the National Bureau of*](#)
663 [Standards 70, no. 4 \(1966\). DOI: jresv70Cn4p263_A1b](#)
664
665 [Kuypers, M. M. M., Marchant, H. K., and Kartal, B.: The microbial nitrogen-cycling network, *Nature Reviews*](#)
666 [Microbiology, 16, 263-276, 2018. DOI: 10.1038/nrmicro.2018.9](#)
667
668 [Laffoley, D., and Baxter, J. M.: Ocean deoxygenation: Everyone's problem: Causes, impacts, consequences and](#)
669 [solutions: Summary for Policy Makers. International Union for Conservation of Nature \(IUCN\), 2019. DOI:](#)
670 [10.2305/IUCN.CH.2019.13.en](#)
671
672 [Li, Yuhong, Yang Luo, Jian Liu, Wangwang Ye, Jiexia Zhang, and Liyang Zhan.: Sources and sinks of N₂O in](#)
673 [the subtropical Jiulong River Estuary, Southeast China. *Frontiers in Marine Science* 10 \(2023\): 1138258. DOI:](#)
674 [10.3389/fmars.2023.1138258](#)
675
676 [Limburg, Karin E., Denise Breitburg, Dennis P. Swaney, and Gil Jacinto.: *Ocean deoxygenation: A primer. One*](#)
677 [Earth 2, no. 1, 2020: 24-29. DOI: 10.1016/j.oneear.2020.01.001](#)
678
679 [Lucieer, V.: *SeaMap Tasmania Bathymetric Data* \[data set\], Institute for Marine and Antarctic Studies,](#)
680 [University of Tasmania, 2007. ISBN: 0-7246-8011-X](#)
681
682 [Ma, X., Lennartz, S. T., and Bange, H. W. : A multi-year observation of nitrous oxide at the Boknis Eck Time](#)
683 [Series Station in the Eckernförde Bay \(southwestern Baltic Sea\). *Biogeosciences*, 16\(20\), 4097-4111, 2019.](#)
684 [DOI: 10.5194/bg-16-4097-2019](#)
685
686 [Macquarie Harbour Dissolved Oxygen Working Group \(October 2014\), Final Report to the Tasmanian Salmonid](#)
687 [Growers Association, 2014.](#)
688
689 [Maher, D. T., J. Z. Sippo, D. R. Tait, C. Holloway, and Santos, I. R.: Pristine mangrove creek waters are a sink](#)
690 [of nitrous oxide. *Scientific Reports*, 6\(25701\), 2016. DOI: 10.1038/srep25701](#)
691
692 [Manning, C. C., Hamme, R. C., & Bourbonnais, A.: Impact of deep-water renewal events on fixed nitrogen loss](#)
693 [from seasonally-anoxic Saanich Inlet. *Marine Chemistry*, 122\(1\), 1–10, 2010. DOI:](#)
694 [10.1016/j.marchem.2010.08.002](#)
695

696 [Maxey, J. D., Hartstein, N. D., Penjinus, D., & Kerroux, A.: Simple quality control technique to identify](#)
697 [dissolved oxygen diffusion issues with biochemical oxygen demand bottle incubations. *Borneo Journal of*](#)
698 [Marine Science and Aquaculture \(BJoMSA\), 1, 2017. DOI: 10.51200/bjomsa.v1i.995](#)
699

700 [Maxey, J. D., Hartstein, N. D., Then, A. Y. H., and Barengeer, M.: Dissolved oxygen consumption in a fjord-like](#)
701 [estuary, Macquarie Harbour, Tasmania. *Estuarine, Coastal and Shelf Science*, 246\(107016\), 2020. DOI:](#)
702 [10.1016/j.ecss.2020.107016](#)
703

704 [Maxey, J. D., Hartstein, N. D., Mujahid, A., & Müller, M.: The influence of mesoscale climate drivers on](#)
705 [hypoxia in a fjord-like deep coastal inlet and its potential implications regarding climate change: examining a](#)
706 [decade of water quality data. *Biogeosciences*, 19\(13\), 3131-3150, 2022. DOI: 10.5194/bg-19-3131-2022](#)
707

708 [McMahon, P. B., and Dennehy, K. F.: N₂O emissions from a nitrogen-enriched river. *Environmental Science &*
709 \[Technology, 33\\(1\\), 21-25, 1999. DOI: 10.1021/es980645n\]\(#\)
710](#)

711 [Michiels, C. C., Huggins, J. A., Giesbrecht, K. E., Spence, J. S., Simister, R. L., Varela, D. E., Hallam, S. J.,](#)
712 [Crowe, S. A.: Rates and pathways of N₂ production in a persistently anoxic fjord: Saanich Inlet, *British*](#)
713 [Columbia. *Frontiers in Marine Science*, 6\(27\), 2019. DOI: 10.3389/fmars.2019.00027](#)
714

715 [Mickett, J. B., Gregg, M. C., and Seim, H. E.: Direct measurements of diapycnal mixing in a fjord reach—Puget](#)
716 [Sound's Main Basin. *Estuarine, Coastal and Shelf Science*, 59\(4\), 539-558, 2004. DOI:](#)
717 [10.1016/j.ecss.2003.10.009](#)
718

719 [Murray, R. H., Erler, D. V., and Eyre, B. D.: Nitrous oxide fluxes in estuarine environments: response to global](#)
720 [change. *Global Change Biology*, 21\(9\), 3219-3245, 2015. DOI: 10.1111/gcb.12923](#)
721

722 [Murray, Rachel, Dirk V. Erler, Judith Rosentreter, Naomi S. Wells, and Bradley D. Eyre.: Seasonal and spatial](#)
723 [controls on N₂O concentrations and emissions in low-nitrogen estuaries: Evidence from three tropical systems.](#)
724 [Marine Chemistry 221 \(2020\): 103779. DOI: 10.1016/j.marchem.2020.103779](#)
725

726 [Musenze, R. S., U. Werner, A. Grinham, J. Udy, and Z. Yuan.: Methane and nitrous oxide emissions from a](#)
727 [subtropical estuary \(the Brisbane River estuary, Australia\). *Science of the Total Environment*, 472, 719–729,](#)
728 [2014. DOI: 10.1016/j.scitotenv.2013.11.085](#)
729

730 [Myhre, G., Shindell, D., Bréon, F. M., Collins, W., Fuglestedt, J., Huang, J., Koch, D., Lamarque, J. F., Lee,](#)
731 [D., Mendoza, B., Nakajima, T., Robock, A., Stephens, G., Takemura, T., and Zhang, H.: Anthropogenic and](#)
732 [Natural Radiative Forcing. In: *Climate Change 2013: The Physical Science Basis. Contribution of Working*](#)
733 [Group I to the Fifth Assessment Report of the Intergovernmental Panel on Climate Change \[Stocker, T.F., Qin,](#)
734 [D., Plattner, G. K., Tignor, M., Allen, S. K., Boschung, J., Nauels, A., Xia, Y., Bex, V., and Midgley, P. M.](#)

735 [\(eds.\)\]. Cambridge University Press, Cambridge, United Kingdom and New York, NY, USA, 2013. DOI:](#)
736 [10.1017/CBO9781107415324.018](#)

737

738 [Myllykangas, J. P., Jilbert, T., Jakobs, G., Rehder, G., Werner, J., and Hietanen, S.: Effects of the 2014 major](#)
739 [Baltic inflow on methane and nitrous oxide dynamics in the water column of the central Baltic Sea. Earth System](#)
740 [Dynamics, 8\(3\), 817-826, 2017. DOI: 10.5194/esd-8-817-2017](#)

741

742 [Nevison, C., and Holland, E.: A reexamination of the impact of anthropogenically fixed nitrogen on atmospheric](#)
743 [N₂O and the stratospheric O₃ layer. Journal of Geophysical Research: Atmospheres, 102\(D21\), 25519-25536,](#)
744 [1997. DOI: 10.1029/97JD02391](#)

745

746 [Orif, M. I., Yasar N. K., Radwan K. A., and Sudheesh, V.: Deoxygenation turns the coastal Red Sea lagoons into](#)
747 [sources of nitrous oxide. Marine Pollution Bulletin 189\(114806\), 2023. DOI: 10.1016/j.marpolbul.2023.114806](#)

748

749 [Portmann, R. W., Daniel, J. S., and Ravishankara, A. R.: Stratospheric ozone depletion due to nitrous oxide:](#)
750 [influences of other gases. Philosophical Transactions of the Royal Society B, 367, 1256–1264, 2012. DOI:](#)
751 [10.1098/rstb.2011.0377](#)

752

753 [Raes, E. J., Bodrossy, L., Van de Kamp, J., Holmes, B., Hardman-Mountford, N., Thompson, P. A., McInnes, A.](#)
754 [S., Waite, A. M.: Reduction of the powerful greenhouse gas N₂O in the South-Eastern Indian Ocean. PLoS One,](#)
755 [11\(1\), 2016. DOI: 10.1371/journal.pone.0145996](#)

756

757 [Ravishankara, A. R., Daniel, J. S., and Portmann, R. W.: Nitrous oxide \(N₂O\): the dominant ozone-depleting](#)
758 [substance emitted in the 21st century. Science, 326\(5949\), 123-125, 2009. DOI: 10.1126/science.1176985](#)

759

760 [Raymond, P. A., and Cole, J. J.: Gas exchange in rivers and estuaries: Choosing a gas transfer velocity.](#)
761 [Estuaries, 24\(2\), 312-317, 2001. DOI: 10.2307/1352954](#)

762

763 [Reading, M. J., Santos, I. R., Maher, D. T., Jeffrey, L. C., and Tait, D. R.: 2017. Shifting nitrous oxide](#)
764 [source/sink behaviour in a subtropical estuary revealed by automated time series observations. Estuarine, Coastal](#)
765 [and Shelf Science, 194: 66-76, 2017. DOI: 10.1016/j.ecss.2017.05.017](#)

766

767 [Reading, M. J., Tait, D. R., Maher, D. T., Jeffrey, L. C., Looman, A., Holloway, C., Shishaye, H. A., Barron, S.](#)
768 [and Santos, I. R.: Land use drives nitrous oxide dynamics in estuaries on regional and global scales. Limnology](#)
769 [and Oceanography, 65\(8\), 1903-1920, 2020. DOI: 10.1002/lno.11426](#)

770

771 [Reading, M.J.: Aquatic nitrous oxide dynamics from rivers to reefs. Doctoral dissertation, Southern Cross](#)
772 [University, 2022. DOI: 10.25918/thesis.197](#)

773

774 [Resplandy, Laure, Allison Hogikyan, Jens Daniel Müller, R. G. Najjar, Hermann W. Bange, Daniele Bianchi, T.](#)
775 [Weber, W.-J. Cai, S. C. Doney, K. Fennel, M. Gehlen, J. Hauck, F. Lacroix, P. Landschützer, C. Le Quéré, A.](#)
776 [Roobaert, J. Schwinger, S. Berthet, L. Bopp, T. T. Chau, M. Dai, N. Gruber, T. Ilyina, A. Kock, M. Manizza,](#)
777 [Z. Lachkar, G. G. Laruelle, E. Liao, I. D. Lima, C. Nissen, C. Rödenbeck, R. Sférian, K. Toyama, H. Tsujino,](#)
778 [P. Regnier.: A synthesis of global coastal ocean greenhouse gas fluxes. Global biogeochemical cycles 38, no. 1](#)
779 [2024: e2023GB007803. DOI: 10.1029/2023GB007803](#)

780

781 [Rönner, U.: Distribution, production and consumption of nitrous oxide in the Baltic Sea. Geochimica et](#)
782 [Cosmochimica Acta, 47\(12\), 2179-2188, 1983. DOI: 10.1016/0016-7037\(83\)90041-8](#)

783

784 [Rosentreter, J. A., Wells, N. S., Ulseth, A. J., and Eyre, B. D.: Divergent gas transfer velocities of CO₂, CH₄, and](#)
785 [N₂O over spatial and temporal gradients in a subtropical estuary. Journal of Geophysical Research:](#)
786 [Biogeosciences, 126\(10\), 2021. DOI: 10.1029/2021JG006270](#)

787

788 [Rosentreter, J.A., Laruelle, G.G., Bange, H.W., Bianchi, T.S., Busecke, J.J., Cai, W.J., Eyre, B.D., Forbrich, I.,](#)
789 [Kwon, E.Y., Maavara, T. and Moosdorf, N.: Coastal vegetation and estuaries are collectively a greenhouse gas](#)
790 [sink. Nature Climate Change, 13\(6\), 579-587, 2023. DOI: 10.1038/s41558-023-01682-9](#)

791

792 [Sánchez-Rodríguez, J., Sierra, A., Jiménez-López, D., Ortega, T., Gómez-Parra, A., and Forja, J.: Dynamic of](#)
793 [CO₂, CH₄ and N₂O in the Guadalquivir estuary. Science of The Total Environment, 805, 2022. DOI:](#)
794 [10.1016/j.scitotenv.2021.150193](#)

795

796 [Schulz, G., Sanders, T., Voynova, Y. G., Bange, H. W., and Dähnke, K.: Seasonal variability of nitrous oxide](#)
797 [concentrations and emissions in a temperate estuary. Biogeosciences, 20\(15\), 3229-3247, 2023. DOI:](#)
798 [10.5194/bg-20-3229-2023](#)

799

800 [Schweiger, B.: Messung von NH₂OH in ausgewählten Seegebieten. Master thesis, Leibniz Institute of Marine](#)
801 [Science, Kiel \(IFM-GEOMAR\), 2006.](#)

802

803 [Seitzinger, S. P., Kroeze, C., and Styles, R. V.: Global distribution of N₂O emissions from aquatic systems:](#)
804 [natural emissions and anthropogenic effects. Chemosphere-Global Change Science, 2\(3-4\), 267-279, 2000. DOI:](#)
805 [10.1016/S1465-9972\(00\)00015-5](#)

806

807 [Sierra, A., Jiménez-López, D., Ortega, T., Gómez-Parra, A., and Forja, J.: Factors controlling the variability and](#)
808 [emissions of greenhouse gases \(CO₂, CH₄ and N₂O\) in three estuaries of the Southern Iberian Atlantic Basin](#)
809 [during July 2017. Marine Chemistry, 226\(103867\), 2020. DOI: 10.1016/j.marchem.2020.103867](#)

810

811 [Salamena, G. G., Whinney, J. C., Heron, S. F., and Ridd, P. V.: Internal tidal waves and deep-water renewal in a](#)
812 [tropical fjord: Lessons from Ambon Bay, eastern Indonesia. Estuarine, Coastal and Shelf Science, 253\(107291\),](#)
813 [2021. DOI: 10.1016/j.ecss.2021.107291](#)

814
815 [Salamena, G. G., Whinney, J. C., Heron, S. F., and Ridd, P. V.: Frontogenesis and estuarine circulation at the](#)
816 [shallow sill of a tropical fjord: Insights from Ambon Bay, eastern Indonesia. *Regional Studies in Marine Science*,](#)
817 [56\(102696\), 2022. DOI: 10.1016/j.rsma.2022.102696](#)
818
819 [Smith, R. W., Bianchi, T. S., Allison, M., Savage, C., and Galy, V.: High rates of organic carbon burial in fjord](#)
820 [sediments globally, *Nature Geoscience*, 8\(6\), 450-453, 2015. DOI: 10.1038/ngeo2421](#)
821
822 [Stow, C. A., Walker, J. T., Cardoch, L., Spence, P., and Geron, C.: N₂O emissions from streams in the Neuse](#)
823 [River watershed, North Carolina. *Environmental Science & Technology*, 39\(18\), 6999-7004, 2005. DOI:](#)
824 [10.1021/es0500355](#)
825
826 [Sturm, K., Werner, U., Grinham, A., and Yuan, Z.: Tidal variability in methane and nitrous oxide emissions](#)
827 [along a subtropical estuarine gradient. *Estuarine, Coastal and Shelf Science*, 192, 159-169, 2017. DOI:](#)
828 [10.1016/j.ecss.2017.04.027](#)
829
830 [Suntharalingam, P., and Sarmiento, J. L.: Factors governing the oceanic nitrous oxide distribution: Simulations](#)
831 [with an ocean general circulation model. *Global Biogeochemical Cycles*, 14\(1\), 429-454, 2000. DOI:](#)
832 [10.1029/1999GB900032](#)
833
834 [Tait, D. R., Maher, D. T., Wong, W., Santos, I. R., Sadat-Noori, M., Holloway, C., and Cook, P. L. M.:](#)
835 [Greenhouse gas dynamics in a salt-wedge estuary revealed by high resolution cavity ringdown spectroscopy](#)
836 [observations. *Environmental Science & Technology*, 51: 13771-13778, 2017. DOI: 10.1021/acs.est.7b04627](#)
837
838 [Tang, Weiyi, Jeff Talbott, Timothy Jones, and Bess B. Ward: Variable contribution of wastewater treatment](#)
839 [plant effluents to downstream nitrous oxide concentrations and emissions. *Biogeosciences* 21, no. 14, 3239-3250,](#)
840 [2024. DOI: 10.5194/bg-21-3239-2024](#)
841
842 [Teasdale, P. R., Apte, S. C., Ford, P. W., Batley, G. E., and Koehnken, L.: Geochemical cycling and speciation](#)
843 [of copper in waters and sediments of Macquarie Harbour, Western Tasmania. *Estuarine, Coastal and Shelf*](#)
844 [Science, 57\(3\), 475-487, 2003. DOI: 10.1016/S0272-7714\(02\)00381-5](#)
845
846 [Testa, Jeremy M., Jacob Carstensen, Arnaud Laurent, and Ming Li.: Hypoxia and Climate Change in Estuaries.](#)
847 [In *Climate Change and Estuaries*, pp. 143-170. CRC Press, 2023. ISBN: 9781003126096](#)
848
849 [Walinsky, S. E., Prah, F. G., Mix, A. C., Finney, B. P., Jaeger, J. M., and Rosen, G. P.: Distribution and](#)
850 [composition of organic matter in surface sediments of coastal Southeast Alaska. *Continental Shelf Research*,](#)
851 [29\(13\), 1565-1579, 2009. DOI: 10.1016/j.csr.2009.04.006](#)
852

853 [Walter, S., Bange, H. W., and Wallace, D. W.: Nitrous oxide in the surface layer of the tropical North Atlantic](#)
854 [Ocean along a west to east transect. *Geophysical Research Letters*, 31\(23\), 2004. DOI: 10.1029/2004GL019937](#)
855

856 [Walter, S., Breitenbach, U., Bange, H. W., Naucsh, G., and Wallace, D. W. R.: Distribution of N₂O in the Baltic](#)
857 [Sea during transition from anoxic to oxic conditions. *Biogeosciences*, 3, 557-570, 2006. DOI: 10.5194/bg-3-557-](#)
858 [2006](#)
859

860 [Wan, X. S., Lin, H., Ward, B. B., Kao, S., and Dai M.: Significant seasonal N₂O dynamics revealed by multi-](#)
861 [year observations in the Northern South China Sea. *Global Biogeochemical Cycles*, 36\(10\), 2022. DOI:](#)
862 [10.1029/2022GB007333](#)
863

864 [Weiss, R. F. and Price, B. A.: Nitrous oxide solubility in water and seawater, *Marine Chemistry*, 8, 347-359,](#)
865 [1980. DOI: 10.1016/0304-4203\(80\)90024-9](#)
866

867 [Wells, N. S., Maher, D. T., Erler, D. V., Hipsey, M., Rosentreter, J. A., and Eyre, B. D.: Estuaries as sources and](#)
868 [sinks of N₂O across a land use gradient in subtropical Australia. *Global Biogeochemical Cycles*, 32, 877–894,](#)
869 [2918. DOI: 10.1029/2017GB005826](#)
870

871 [Willis, M.: Tascatch Variation 2 – Surface Water Models \(Document ID Number WR 2008/005\). Department of](#)
872 [Primary Industries and Water. Hydro Tasmania Consulting, \[https://nre.tas.gov.au/water/water-monitoring-and-\]\(https://nre.tas.gov.au/water/water-monitoring-and-assessment/hydrological%20assessment/tasmanian-catchmentsmodelling/surface-water-models\)](#)
873 [assessment/hydrological%20assessment/tasmanian-catchmentsmodelling/surface-water-models](#). 2008.
874

875 [Wilson, S. T., Bange, H. W., Arévalo-Martínez, D. L., Barnes, J., Borges, A. V., Brown, I., Bullister, J. L.,](#)
876 [Burgos, M., Capelle, D. W., Casso, M., de la Paz, M., Farías, L., Fenwick, L., Ferrón, S., Garcia, G., Glockzin,](#)
877 [M., Karl, D. M., Kock, A., Laperriere, S., Law, C. S., Manning, C. C., Marriner, A., Myllykangas, J. P., Pohlman,](#)
878 [J. W., Rees, A. P., Santoro, A. E., Tortell, P. D., Upstill-Goddard, R. C., Wisegarver, D. P., Zhang, G. L., and](#)
879 [Rehder, G.: An intercomparison of oceanic methane and nitrous oxide measurements, *Biogeosciences*, 15, 5891-](#)
880 [5907, 2018. DOI: 10.5194/bg-15-5891-2018](#)
881

882 [Wilson, S. T., Al-Haj, A. N., Bourbonnais, A., Frey, C., Fulweiler, R. W., Kessler, J. D., Marchant, H. K.,](#)
883 [Milucka, J., Ray, N. E., Suntharalingham, P., Thornton, B. F., Upstill-Goddard, R. C., Weber, T. S., Arévalo-](#)
884 [Martínez, D. L., Bange, H. W., Benway, H. M., Bianchi, D., Borges, A. V., Chang, B. X., Crill, P. M., del Valle,](#)
885 [D. A., Farías, L., Joye, S. B., Kock, A., Labidi, J., Manning, C. C., Pohlman, J. W., Rehder, G., Sparrow, K. J.,](#)
886 [Tortell, P. D., Treude, T., Valentine, D. L., Ward B. B., Yang, S., and Yurganov, L. N.: Ideas and perspectives:](#)
887 [A strategic assessment of methane and nitrous oxide measurements in the marine environment. *Biogeosciences*,](#)
888 [17, 5809-5828, 2020. DOI: 10.5194/bg-17-5809-2020](#)
889

890 [Wu, L., Chen X., Wei, W., Liu, Y., Wang, D., and Ni, B.: A critical review on nitrous oxide production by](#)
891 [ammonia-oxidizing archaea. *Environmental Science & Technology* 54\(15\), 9175-9190, 2020. DOI:](#)
892 [10.1021/acs.est.0c03948](#)

893
894 [Yevenes, M. A., Bello, E., Sanhueza-Guevara, S., and Farías, L.: Spatial distribution of nitrous oxide \(N₂O\) in](#)
895 [the Reloncaví estuary–sound and adjacent sea \(41–43 S\), Chilean Patagonia. *Estuaries and Coasts*, 40, 807-821,](#)
896 [2017. DOI: 10.1007/s12237-016-0184-z](#)

897
898 [Yoshinari, T.: Nitrous oxide in the sea. *Marine Chemistry* 2\(4\), 189–202, 1976. DOI: 10.1016/0304-](#)
899 [4203\(76\)90007-4.](#)

900
901 [Zappa, C. J., Raymond, P. A., Terray, E. A., and McGillis, W. R.: Variation in surface turbulence and the gas](#)
902 [transfer velocity over a tidal cycle in a macro-tidal estuary. *Estuaries*, 26, 1401-1415, 2003. DOI:](#)
903 [10.1007/BF02803649](#)

904
905 [Zhang, G. L., Zhang, J., Liu, S. M., Ren, J. L., and Zhao, Y. C.: Nitrous oxide in the Changjiang \(Yangtze](#)
906 [River\) Estuary and its adjacent marine area: Riverine input, sediment release and atmospheric fluxes.](#)
907 [Biogeosciences 7\(11\), 3505-3516, 2010. DOI: 10.5194/bg-7-3505-2010](#)

908 [Zhang, G. L., Zhang, J., Liu, S. M., Ren, J. L., and Zhao, Y. C.: Nitrous oxide in the Changjiang \(Yangtze\)](#)
[River\) Estuary and its adjacent marine area: Riverine input, sediment release and atmospheric fluxes.](#)
[Biogeosciences 7\(11\), 3505-3516, 2010. DOI: 10.5194/bg-7-3505-2010](#)